Available online at www.sciencedirect.com
ScienceDirect
Journal of Computational Physics 227 (2008) 1676–1700
JOURNAL OF COMPUTATIONAL PHYSICS
www.elsevier.com/locate/jcp

Reduced aliasing formulations of the convective terms within the Navier–Stokes equations for a compressible fluid

Christopher A. Kennedy [a,*], Andrea Gruber [b]

[a] Bechtel National Inc., 50 Beale St., San Francisco, CA 94105, USA
[b] SINTEF Energy Research, Sem Saelandsvei 11, 7465 Trondheim, Norway

Received 4 January 2007; received in revised form 23 September 2007; accepted 25 September 2007
Available online 6 October 2007

Abstract

The effect on aliasing errors of different formulations describing the cubically nonlinear convective terms within the discretized Navier–Stokes equations is examined in the presence of a non-trivial density spectrum. Fourier analysis shows that the existing skew-symmetric forms of the convective term result in reduced aliasing errors relative to the conservation form. Several formulations of the convective term, including a new formulation proposed for cubically nonlinear terms, are tested in direct numerical simulation (DNS) of decaying compressible isotropic turbulence both in chemically inert (small density fluctuations) and reactive cases (large density fluctuations) and for different degrees of resolution. In the DNS of reactive turbulent flow, the new cubic skew-symmetric form gives the most accurate results, consistent with the spectral error analysis, and at the lowest cost. In marginally resolved DNS and LES (poorly resolved by definition) the new cubic skew-symmetric form represents a robust convective formulation which minimizes both aliasing and computational cost while also allowing a reduction in the use of computationally expensive high-order dissipative filters.
© 2007 Elsevier Inc. All rights reserved.

PACS: 65T99; 76N10

Keywords: Navier–Stokes equations; Compressible flows; Convective operators; Skew-symmetric form; Aliasing

1. Introduction

Numerical simulations of the Navier–Stokes equations (NSE) for a compressible, reactive fluid are unavoidably plagued with some degree of error. Error sources include the truncation error associated with the integration and differentiation, round-off error, and error in the specification of the boundary conditions. Another important source of error is aliasing error [3,4] which arises during the differentiation of the product of two (or more) variables. This is particularly important in the evaluation of the convective terms of the Navier–Stokes equations. Aliasing error is present in pseudospectral, finite-difference, finite-volume, and finite-element approaches both in LES and DNS of turbulent flows. The aliasing phenomenon is often

* Corresponding author. Tel.: +1 415 768 1228; fax: +1 415 768 1794.
E-mail address: cakenned@bechtel.com (C.A. Kennedy).

0021-9991/$ - see front matter © 2007 Elsevier Inc. All rights reserved.
doi:10.1016/j.jcp.2007.09.020

manifested by an unphysical growth of the spectral energy content of the integration variables at high wavenumbers. This energy growth at the high wavenumber end of the spectrum is accompanied by an equally artificial and accelerated decay of the energy content at the low wavenumber end of the spectrum. In situations where they are available, purely dissipative, high-order filters [15,19,23] may be used to remove the aliased energy accumulated at the highest wavenumbers of the spectrum. However, this technique does not compensate for the spectral energy loss at the low wavenumber modes. Therefore, it is generally prudent to select a numerical scheme which minimizes energy aliasing from the convection operator. In doing so, the need for high-order, dissipative filters will be minimized. Using minimally aliasing convection operators is particularly important in contexts where good filters are not readily available or there is little inherent dissipation in the numerical method. Low-order methods, with their high inherent dissipation, will likely see less benefit from better convection operators than higher-order methods. As there are other sources of high wavenumber information on the computational grid such as inexact derivative operators, high-order, dissipative filters are still an important tool in simulations of the NSE, when available.

Efforts to reduce aliasing error associated with the convective discretization of the NSE have their origin in constant density contexts [11] where the nonlinearities encountered in the convective terms are quadratic. Zang [29] performs tests to compare the four alternative formulations of the convective terms in the incompressible NSE: conservation/divergence, convection, rotation, and skew-symmetric. Subsequent to this, Horiuti and Itami [13], and Kravchenko and Moin [18] consider constant density flows while Blaisdell et al. [1,2], Chow and Moin [5], Ducros et al. [6], and Morinishi et al. [22] consider variable density flows. It is generally recognized that the aliasing error, for both constant and variable density flows, can be minimized by using a skew-symmetric formulation of the convective terms, however Boyd [3] importantly remarks that, if nonlinear interactions are so strong that non-trivial amounts of energy are being aliased, then the number of grid points should be increased in order to produce a meaningful solution. Other works on aliasing in simulations of an incompressible fluid may be found in the papers of Wilhelm and Kleiser [28], Lube and Olshanskii [21], Verstappen and Veldman [27], and Park and Mahesh [24].

In variable density flows, the convective terms are characterized by cubic nonlinearities and it is unclear whether one may simply recast a cubically nonlinear term using constructs specifically designed for quadratic nonlinearities [1,2,5,6,22]. Additionally, there is an inherent ambiguity in applying a skew-symmetric formulation constructed for quadratic nonlinearities to a cubically nonlinear term; three formulations are possible, two of which are mentioned in the open literature [1,9]. It should be stressed that if the density field is characterized by very small fluctuations and, consequently, it has no meaningful spectrum, then the variable density case will resemble the constant density case with quadratic nonlinearities. However, in compressible, multicomponent, reacting flows, the density will generally have a relatively broad spectrum. The objective of the paper is to explore a wide range of convective formulations that, to varying degrees, minimize aliasing error for quadratically and cubically nonlinear terms and to verify the robustness of these formulations in cases of a non-trivial density spectrum.

2. Background

The dimensional form of the Navier–Stokes equations for a compressible, multicomponent, reacting fluid is given by the following expressions:

$$\frac{\partial(\rho \mathbf{u}_i)}{\partial t} + \nabla_j \cdot (\rho \mathbf{u}_i \mathbf{u}_j) = \nabla_j \cdot (-p\delta_{ij} + \boldsymbol{\tau}_{ji}) + \rho \sum_{s=1}^{N_g} Y_s \mathbf{f}_{si} \tag{1}$$

$$\frac{\partial \rho}{\partial t} + \nabla_j \cdot (\rho \mathbf{u}_j) = 0 \tag{2}$$

$$\frac{\partial(\rho e_0)}{\partial t} + \nabla_j \cdot (\rho e_0 \mathbf{u}_j) = \nabla_j \cdot (-p\mathbf{u}_j + \boldsymbol{\tau}_{ji} \cdot \mathbf{u}_i - \mathbf{q}_j) + \rho \mathbf{u}_j \cdot \sum_{s=1}^{N_g} Y_s \mathbf{f}_{sj} + \sum_{s=1}^{N_g} \mathbf{f}_{sj} \cdot \mathbf{J}_{sj} \tag{3}$$

$$\frac{\partial(\rho Y_s)}{\partial t} + \nabla_j \cdot (\rho Y_s \mathbf{u}_j) = -\nabla_j \cdot \mathbf{J}_{sj} + W_s \dot{\omega}_s \tag{4}$$

where $i,j = 1,2,3$, ρ is the density, p is the pressure, e_0 is total specific internal energy, $s = 1,2,\ldots,N_g$ is the species index, N_g is the total number of species, Y_s is the mass fraction of species s, t is the time, i and j are spatial direction indices, $\mathbf{u}_i$ is the velocity vector component in direction i, $\mathbf{f}_{si}$ is the body force per unit mass of species s in direction i, $\mathbf{J}_{si} = \rho Y_s \mathbf{V}_{si}$ is the diffusive flux of species s in direction i, $\mathbf{V}_{si}$ is the diffusion velocity of species s in direction i, $\mathbf{q}_j$ is the heat flux vector in direction j, $\boldsymbol{\tau}_{ji}$ is the transpose of the viscous stress tensor for directions i and j, $\dot{\omega}_s$ is the molar reaction rate of species s per unit volume, and ∇_j is the gradient operator in direction j. The particular form given above is that commonly found from a continuum derivation of the expressions for mass, momentum, energy, and species mass balance relations in integral form. Though not given, an equation of state for the fluid is also required to integrate the governing equations.

While the Einstein summation convention is used, a dot product symbol is included to emphasize both the divergence and directional derivative operators, when appropriate. The particular choices of constitutive models for $\mathbf{q}_j$, $\mathbf{V}_{sj}$, $\boldsymbol{\tau}_{ij}$, and $\dot{\omega}_s$ are not immediately relevant to the results of this paper. However, to correctly account for the relative operations count of each possible convective operator, it will be assumed that gradients of chemical species computed for $\mathbf{J}_{si}$ are available to any convective operator that needs these terms. No attempt will be made to reformulate the divergence of the viscous fluxes: $\nabla \cdot \boldsymbol{\tau}^T$, $\nabla \cdot \mathbf{q}$ and $\nabla \cdot \mathbf{J}$. Rather, this paper focuses only on how one best discretizes the quadratically nonlinear $\nabla_j \cdot (\rho \mathbf{u}_j)$, $\nabla_j \cdot (p\mathbf{u}_j)$, and cubically nonlinear $\nabla_j \cdot (\rho \mathbf{u}_i \mathbf{u}_j)$, $\nabla_j \cdot (\rho e_0 \mathbf{u}_j)$, and $\nabla_j \cdot (\rho Y_s \mathbf{u}_j)$ terms so as to minimize aliasing error generated during numerical simulations.

In what follows, inviscid components of (1)–(4) will be manipulated for the purposes of reducing aliasing errors. Although the equations are expressed in what is often called primitive variables, a different set of variables may be chosen. On the other hand, awkward choices for the integration variables will likely complicate the solution procedure and are of questionable value when solving for flows which are not single-component, ideal gases having constant properties. In this paper, convective formulations are constructed using only primitive variables because they are a natural choice and they readily facilitate symmetrical groupings of variables.

2.1. Convective formulations

If one focuses on the terms on the left-hand side (LHS) of (1)–(4), one may write these terms in several analytically equivalent forms. The essential point, and the motivation for this paper, is that these mathematically equivalent forms are not numerically equivalent. For the momentum and scalar, $\phi = \{1, e_0, Y_s\}$, equations, one can write the four traditional forms: the *divergence* or *conservation* form

$$\frac{\partial(\rho \mathbf{u}_i)}{\partial t} + \nabla_j \cdot (\rho \mathbf{u}_i \mathbf{u}_j) = \mathrm{RHS}_{\rho \mathbf{u}} \tag{5}$$

$$\frac{\partial(\rho \phi)}{\partial t} + \nabla_j \cdot (\rho \phi \mathbf{u}_j) = \mathrm{RHS}_{\phi} \tag{6}$$

the *convection* form

$$\rho \frac{\partial \mathbf{u}_i}{\partial t} + \rho \mathbf{u}_j \cdot (\nabla_j \mathbf{u}_i) = \mathrm{RHS}_{\rho \mathbf{u}} \tag{7}$$

$$\rho \frac{\partial \phi}{\partial t} + \rho \mathbf{u}_j \cdot \nabla_j \phi = \mathrm{RHS}_{\phi} \tag{8}$$

the *skew-symmetric* forms $\mathrm{QSS_F}$

$$\frac{\partial(\rho \mathbf{u}_i)}{\partial t} + \frac{1}{2}\left[\nabla_j \cdot (\rho \mathbf{u}_i \mathbf{u}_j) + \rho \mathbf{u}_j \cdot (\nabla_j \mathbf{u}_i) + \mathbf{u}_i \nabla_j \cdot (\rho \mathbf{u}_j)\right] = \mathrm{RHS}_{\rho \mathbf{u}} \tag{9}$$

$$\frac{\partial(\rho \phi)}{\partial t} + \frac{1}{2}\left[\nabla_j \cdot (\rho \phi \mathbf{u}_j) + \rho \mathbf{u}_j \cdot \nabla_j \phi + \phi \nabla_j \cdot (\rho \mathbf{u}_j)\right] = \mathrm{RHS}_{\phi} \tag{10}$$

and $\mathrm{QSS_B}$

$$\frac{\partial(\rho \mathbf{u}_i)}{\partial t} + \frac{1}{2}\left[\nabla_j \cdot (\rho \mathbf{u}_i \mathbf{u}_j) + \rho \mathbf{u}_i (\nabla_j \cdot \mathbf{u}_j) + \mathbf{u}_j \cdot \nabla_j (\rho \mathbf{u}_i)\right] = \mathrm{RHS}_{\rho \mathbf{u}} \tag{11}$$

$$\frac{\partial(\rho\phi)}{\partial t}+\frac{1}{2}[\nabla_j\cdot(\rho\phi\mathbf{u}_j)+\rho\phi(\nabla_j\cdot\mathbf{u}_j)+\mathbf{u}_j\cdot\nabla_j(\rho\phi)]=\mathrm{RHS}_\phi \tag{12}$$

where for constant density flows, the two momentum forms, (9) and (11), and the two scalar forms, (10) and (12), become identical. Note that there is a difference in how (10) and (12) simplify to the continuity equation by setting $\phi=1$. Only (12) produces a formulation different from the conservation form,

$$\frac{\partial\rho}{\partial t}+\frac{1}{2}[\nabla_j\cdot(\rho\mathbf{u}_j)+\rho(\nabla_j\cdot\mathbf{u}_j)+\mathbf{u}_j\cdot\nabla_j\rho]=\mathrm{RHS}_\phi \tag{13}$$

Feiereisen et al. [9] employ (9) while Blaisdell et al. [1,2] use (11). In the next sections, (9) and (10) will be named the *Feiereisen quadratic skew-symmetric formulation* or, $\mathrm{QSS_F}$, while (11) and (12) will be named the *Blaisdell quadratic skew-symmetric formulation* or, $\mathrm{QSS_B}$. Erlebacher and Hussaini [7] state that simulations of supersonic boundary layer transition were stable using (9) but not (11). The ambiguity in the definition for a skew-symmetric convective operator in the compressible case is a consequence of a cubically nonlinear term being treated as a quadratically nonlinear term. Another consequence of this ambiguity is that quadratic skew-symmetric formulations of the momentum equation using momentum and velocity as the two groups of variables may be written in two different ways; $\mathrm{QSS_B}$ and $\mathrm{QSS_F}$.

One further way to apply the derivative of a product, though not necessarily toward a useful construct, is

$$\frac{\partial(\rho\mathbf{u}_i)}{\partial t}+\frac{1}{2}[\nabla_j\cdot(\rho\mathbf{u}_i\mathbf{u}_j)+\mathbf{u}_i\mathbf{u}_j\cdot(\nabla_j\rho)+\rho\nabla_j\cdot(\mathbf{u}_i\mathbf{u}_j)]=\mathrm{RHS}_{\rho\mathbf{u}} \tag{14}$$

$$\frac{\partial(\rho\phi)}{\partial t}+\frac{1}{2}[\nabla_j\cdot(\rho\phi\mathbf{u}_j)+\phi\mathbf{u}_j\cdot(\nabla_j\rho)+\rho\nabla_j\cdot(\phi\mathbf{u}_j)]=\mathrm{RHS}_\phi \tag{15}$$

This convective operator could potentially find use in flows with relatively narrow velocity spectra yet broad density spectra. Morinishi et al. [22] also include another variation on skew-symmetry by combining (11) or (12) with the continuity equation

$$\rho\frac{\partial\mathbf{u}_i}{\partial t}+\frac{1}{2}[\nabla_j\cdot(\rho\mathbf{u}_i\mathbf{u}_j)-\mathbf{u}_i\nabla_j\cdot(\rho\mathbf{u}_j)+\rho\mathbf{u}_j\cdot(\nabla_j\mathbf{u}_i)]=\mathrm{RHS}_{\rho\mathbf{u}} \tag{16}$$

$$\rho\frac{\partial\phi}{\partial t}+\frac{1}{2}[\nabla_j\cdot(\rho\phi\mathbf{u}_j)-\phi\nabla_j\cdot(\rho\mathbf{u}_j)+\rho\mathbf{u}_j\cdot(\nabla_j\phi)]=\mathrm{RHS}_\phi \tag{17}$$

Honein and Moin [12] consider a skew-symmetric form of the total energy equation

$$\begin{aligned}&\frac{\partial(\rho e_0)}{\partial t}+\mathbf{u}_i\cdot[\nabla_j\cdot(\rho\mathbf{u}_i\mathbf{u}_j)]+(\rho\mathbf{u}_i\mathbf{u}_j):(\nabla_i\mathbf{u}_j)+\frac{1}{2}\nabla_j\cdot(\rho e_0\mathbf{u}_j)+\frac{e}{2}\nabla_j\cdot(\rho\mathbf{u}_j)+\frac{\rho\mathbf{u}_j}{2}\cdot(\nabla_j e)+p(\nabla_j\cdot\mathbf{u}_j)\\&\quad+(\mathbf{u}_j\cdot\nabla_j)p=\mathbf{u}_i\cdot(\nabla_j\cdot\boldsymbol{\tau}_{ji})+\boldsymbol{\tau}_{ji}:(\nabla_i\mathbf{u}_j)-\nabla_j\cdot\mathbf{q}_j+\rho\mathbf{u}_j\cdot\sum_{s=1}^{N_g}Y_s\mathbf{f}_{sj}+\sum_{s=1}^{N_g}\mathbf{f}_{sj}\cdot\mathbf{J}_{sj}\end{aligned} \tag{18}$$

where body force terms have been added to be consistent with (3) and e denotes the specific internal energy.

Lastly, one has the *rotation* form

$$\frac{\partial(\rho\mathbf{u}_i)}{\partial t}+\rho\left[(\omega\times\mathbf{u})_i+\frac{1}{2}\nabla_i(\mathbf{u}_j\cdot\mathbf{u}_j)\right]+\mathbf{u}_i\nabla_j\cdot(\rho\mathbf{u}_j)=\mathrm{RHS}_{\rho\mathbf{u}} \tag{19}$$

where there is no *rotation* form for scalar evolution equations. Fedioun et al. [8] include a variation on (19) where $(1/2)\nabla_i(\mathbf{u}_j\cdot\mathbf{u}_j)=(\nabla_i\mathbf{u}_j)\cdot\mathbf{u}_j$. Many other analytically equivalent expressions of the governing equations may be readily derived.

2.2. An improved "skew-symmetric" formulation

2.2.1. Quadratic nonlinearities

As a prelude to the analysis of cubically nonlinear terms, reviewing the analysis of quadratically nonlinear terms is useful. Blaisdell et al. [1,2] have derived a convenient way to express conservation (5 and 6), convection (7 and 8) and skew-symmetric (9)–(12) forms in the following single generalized expression

$$\nabla(fg) = \alpha\nabla(fg) + (1-\alpha)[g\nabla f + f\nabla g] \tag{20}$$

however, in spirit and origin, the above expression is restricted to quadratic nonlinearities. By this, it is meant that neither f nor g may be further decomposed into the product of other variables. Note that the form of (20) expresses the derivative of a product in terms of symmetrical groupings of all possible equivalent terms computed as the derivative of a product. The coefficient $\alpha = 0, 1/2, 1$ corresponds to the convection, skew-symmetric, and conservation forms, respectively. Defining the Fourier transforms

$$f(x) = \sum_{p=-\frac{N}{2}+1}^{\frac{N}{2}} \hat{f}_p \mathrm{e}^{\mathrm{i}k_p x}, \quad g(x) = \sum_{q=-\frac{N}{2}+1}^{\frac{N}{2}} \hat{g}_q \mathrm{e}^{\mathrm{i}k_q x} \tag{21}$$

$$f(x)g(x) = \sum_{p,q=-\frac{N}{2}+1}^{\frac{N}{2}} \sum^{\frac{N}{2}} \hat{f}_p \hat{g}_q \mathrm{e}^{\mathrm{i}(k_p+k_q)x} \tag{22}$$

the derivative of $f(x)g(x)$ evaluated at the gridpoint l is

$$\left.\frac{\partial\{f(x)g(x)\}}{\partial x}\right|_l = \sum_{p,q=-\frac{N}{2}+1}^{\frac{N}{2}} \sum^{\frac{N}{2}} i(k_p+k_q)\hat{f}_p\hat{g}_q \mathrm{e}^{\mathrm{i}(k_p+k_q)x_l} \tag{23}$$

where modes $-N/2$ and $N/2$ define the wavenumber range that the numerical grid is able to resolve. Substituting this expression into the generalized convective term in (20), one obtains

$$\left.\frac{\partial\{f(x)g(x)\}}{\partial x}\right|_l = \sum_{p,q=-\frac{N}{2}+1}^{\frac{N}{2}} \sum^{\frac{N}{2}} ik^*\hat{f}_p\hat{g}_q \mathrm{e}^{\mathrm{i}(k_p+k_q)x_l} \tag{24}$$

where

$$k^* = \{\alpha(k_p+k_q)^{\diamondsuit} + (1-\alpha)(k_p+k_q)\} \tag{25}$$

will be referred to as effective amplitude (or modified) wavenumber because it is the wavenumber associated with the wave amplitude $k^*\hat{f}_p\hat{g}_q$. This is to be contrasted with the correct amplitude $(k_p+k_q)\hat{f}_p\hat{g}_q$. The wavenumbers denoted with a superscript $^{\diamondsuit}$ in (25) arise from the quadratic term (first term on the right-end side) of (20) while the linear terms of (20) result in the wavenumber with no superscripts. To make the analysis more productive, each wavenumber will be chosen to be the same so that neither of the variables (g or f) has precedence over the other. Hence, $k_p = k_q$ in the quadratic case giving

$$k^* = \{\alpha(k_p+k_p)^{\diamondsuit} + (1-\alpha)(k_p+k_p)\} \tag{26}$$

In the case of quadratic nonlinearities, for $|2k_p| \leqslant N/2$, there is no aliasing of wavenumbers. However, for $N/2 < |2\ k_p| \leqslant N$, the true wavenumber sums $(N/2+\xi)$ and $(-N/2-\ \xi)$ are aliased by the quadratic term to $2k = (-N/2+\xi)$ and $2k^{\diamondsuit} = (N/2-\xi)$, respectively. Focusing only on positive k, one has that $\xi = 2k_p - N/2$, where the quantity ξ describes the "distance" of the unresolved wavenumber $2k_p > N/2$ from the resolved range. Consequently, the modified wavenumber k^* in this quadratic case can be expressed by substituting these terms into (26) to find

$$k^* = \alpha\left(\frac{-N}{2}+\xi\right) + (1-\alpha)\left(\frac{N}{2}+\xi\right) = \frac{(1-2\alpha)N}{2} + \xi = c_1 \tag{27}$$

where c_1 is simply k^* outside the resolved range for $N/2\ < 2k_p \leqslant N$. Therefore, the modified wavenumber may be expressed in terms of the true wavenumber for the entire positive range of wavenumbers as

$$\begin{aligned} k^* &= k, \quad 0 \geqslant k \geqslant \frac{N}{2} \\ k^* &= \frac{-N}{2} + \frac{(1-2\alpha)N}{2} + k, \quad \frac{N}{2} < k \geqslant N \end{aligned} \tag{28}$$

While the aliasing errors described by k^* cannot be removed, it is generally advisable to employ the convective formulation that minimizes the value of k^* when $2k_p$ is not resolved by the grid. Table 1 shows the values of $c_1 = k^*$ for several convective formulations. In Fig. 1, k^* versus k is plotted for each of these formulations. Ideally, $k^* \approx 0$ would be enforced for all aliased wavenumbers but this is not possible. Since it is likely that most integration variables will have a decaying spectrum as wavenumbers increase, having $k^* \approx 0$ at lower wavenumbers would mean less wavenumber energy available for aliasing. Hence, to optimize the convective operator, $k^* = 0$ is chosen at the lowest wavenumber for a given aliasing regime. For the quadratic operator, $k = N/2$ is chosen and then $k^* = 0$ implies $\alpha = 1/2$. This choice is most likely to minimize aliased wavenumber energy and corresponds to the skew-symmetric forms $\mathrm{QSS_F}$ and $\mathrm{QSS_B}$.

2.2.2. Cubic nonlinearities

For cubic nonlinearities such as $\nabla_j \cdot (\rho \mathbf{u}_i \mathbf{u}_j)$, $\nabla_j \cdot (\rho e_0 \mathbf{u}_j)$, and $\nabla_j \cdot (\rho Y_s \mathbf{u}_j)$, one may begin extending (20) by taking the gradient of three variables: f,g, and h. One is free to then write

$$\nabla(fgh) = \alpha\nabla(fgh) + \beta\nabla(fgh) + \gamma\nabla(fgh) + \delta\nabla(fgh) + \epsilon\nabla(fgh) \tag{29}$$

where $\epsilon = (1 - \alpha - \beta - \gamma - \delta)$. Next, by differentiating a product, the original terms may be written in four different yet analytically equivalent forms:

Table 1
Coefficients of (20) where $\beta = (1 - \alpha)$ along with the associated values of $k^* = c_1$

Case	α	β	c_1
2	α	β	$\frac{(1-2\alpha)N}{2} + \xi$
2a	1	0	$\frac{-N}{2} + \xi$
2b	$\frac{3}{4}$	$\frac{1}{4}$	$\frac{-N}{4} + \xi$
2c	$\frac{1}{2}$	$\frac{1}{2}$	ξ
2d	$\frac{1}{4}$	$\frac{3}{4}$	$\frac{N}{4} + \xi$
2e	0	1	$\frac{N}{2} + \xi$

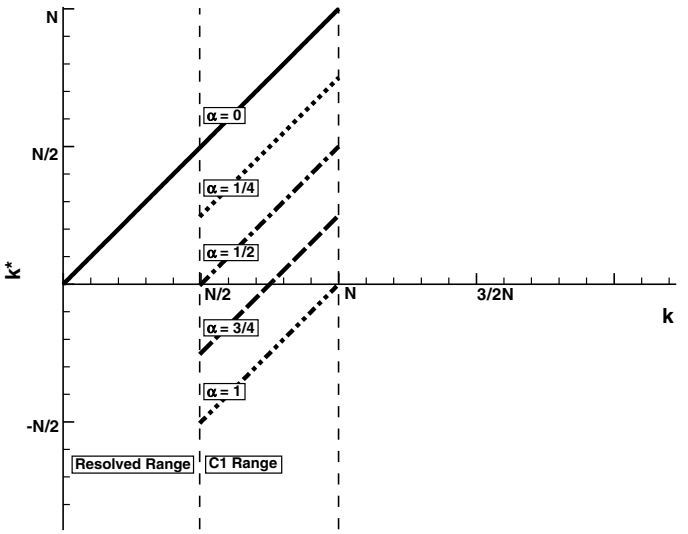

Fig. 1. Modified wavenumber $k^* = c_1$ versus k for different values of α in quadratic skew-symmetric formulations.

$$\nabla(fgh) = f\nabla(gh) + gh\nabla f = g\nabla(fh) + fh\nabla g = h\nabla(fg) + fg\nabla h = gh\nabla f + fh\nabla g + fg\nabla h \tag{30}$$

Substituting each of these five terms into (29) once gives

$$\begin{aligned}\nabla(fgh) = {} & \alpha\nabla(fgh) + \beta[f\nabla(gh) + gh\nabla f] + \gamma[g\nabla(fh) + fh\nabla g] + \delta[h\nabla(fg) + fg\nabla h] + \epsilon[gh\nabla f \\ & + fh\nabla g + fg\nabla h]\end{aligned} \tag{31}$$

Setting $\beta = \gamma = \epsilon = 0$, the conservation, skew-symmetric and convective forms correspond to $(\alpha = 1, \delta = 0)$, $(\alpha = 1/2, \delta = 1/2)$, and $(\alpha = 0, \delta = 1)$, respectively. Collecting terms in (31),

$$\nabla(fgh) = \alpha\nabla(fgh) + \beta f\nabla(gh) + \gamma g\nabla(fh) + \delta h\nabla(fg) + (\beta + \epsilon)gh\nabla f + (\gamma + \epsilon)fh\nabla g + (\delta + \epsilon)fg\nabla h \tag{32}$$

Organizing the quadratic and linear terms into symmetrical groupings in analogy with the constant density, skew-symmetric form, one may set $\beta = \gamma = \delta$ so that $\epsilon = (1 - \alpha - 3\beta)$ giving equal weight to different permutations of the variables. This gives

$$\nabla(fgh) = \alpha\nabla(fgh) + \beta[f\nabla(gh) + g\nabla(fh) + h\nabla(fg)] + (1 - \alpha - 2\beta)[gh\nabla f + fh\nabla g + fg\nabla h] \tag{33}$$

For $\alpha = 1$ and $\beta = 0$, one gets the conservation form. One can no longer retrieve any of the quadratic skew-symmetric or convection forms after having set $\beta = \gamma = \delta$. Setting $\beta = 0$ and $h = 1$ in (33), (20) is retrieved. Note that the coefficient α multiplies the cubic term, β multiplies the quadratic term, and $(1 - \alpha - 2\beta)$ multiplies the linear term. Next, the functions $f(x)$, $g(x)$, and $h(x)$ may be expanded as was done in (21)

$$\begin{aligned} f(x) &= \sum_{p=-\frac{N}{2}+1}^{\frac{N}{2}} \hat{f}_p e^{ik_p x} \\ g(x) &= \sum_{q=-\frac{N}{2}+1}^{\frac{N}{2}} \hat{g}_q e^{ik_q x} \\ h(x) &= \sum_{r=-\frac{N}{2}+1}^{\frac{N}{2}} \hat{h}_r e^{ik_r x} \end{aligned} \tag{34}$$

Their product is then given by

$$f(x)g(x)h(x) = \sum_{p,q,r=-\frac{N}{2}+1}^{\frac{N}{2}} \hat{f}_p \hat{g}_q \hat{h}_r e^{i(k_p+k_q+k_r)x} \tag{35}$$

while the derivative of this product at grid point l is

$$\left.\frac{\partial\{f(x)g(x)h(x)\}}{\partial x}\right|_l = \sum_{p,q,r=-\frac{N}{2}+1}^{\frac{N}{2}} i(k_p + k_q + k_r)\hat{f}_p \hat{g}_q \hat{h}_r e^{i(k_p+k_q+k_r)x_l} \tag{36}$$

Substituting the generalized convective term, (33), into this expression gives

$$\left.\frac{\partial\{f(x)g(x)h(x)\}}{\partial x}\right|_l = \sum_{p,q,r=-\frac{N}{2}+1}^{\frac{N}{2}} ik^* \hat{f}_p \hat{g}_q \hat{h}_r e^{i(k_p+k_q+k_r)x_l} \tag{37}$$

where

$$k^* = \alpha(k_p + k_q + k_r)^\circ + \beta[(k_q + k_r)^\diamond + (k_p + k_r)^\diamond + (k_p + k_q)^\diamond] + (1 - \alpha - 2\beta)(k_p + k_q + k_r) \tag{38}$$

Terms denoted with a superscript $^\circ$ arise from cubically nonlinear terms while those denoted with the superscript $^\diamond$ are from quadratically nonlinear terms. Setting $k_p = k_q = k_r$ so that neither of the variables (g, h, or f) has precedence over the others, the modified wavenumber can be expressed as

$$k^* = \alpha(k_p + k_p + k_p)^\circ + 3\beta(k_p + k_p)^\diamond + (1 - \alpha - 2\beta)(k_p + k_p + k_p) \tag{39}$$

When cubic nonlinearities are present, the spectral aliasing analysis involves two different aliasing regimes, rather than only one aliasing regime as in the quadratically nonlinear case. The first aliasing regime is when only the cubic term aliases and this is the case for $3k_p > N/2$ but $2k_p \leqslant N/2$ or $3k_p \leqslant 3N/4$. Hence, $3k_p = N/2 + \xi$ and

$$\begin{aligned}(k_p + k_p + k_p) &= \left(\frac{N}{2} + \xi\right)\\ (k_p + k_p)^\diamond &= \frac{2}{3}\left(\frac{N}{2} + \xi\right)\\ (k_p + k_p + k_p)^\circ &= \left(\frac{-N}{2} + \xi\right)\end{aligned} \tag{40}$$

and therefore (39) becomes

$$k^* = \alpha\left(\frac{-N}{2} + \xi\right) + 2\beta\left(\frac{N}{2} + \xi\right) + (1 - \alpha - 2\beta)\left(\frac{N}{2} + \xi\right) = c_1 \tag{41}$$

where c_1 is k^* for $N/2 < 3k_p \leqslant 3N/4$. Since the most common aliasing occurrence will be that the sum of all three wavenumbers will exceed $|N/2|$ rather than the sum of any two, it is the c_1 term that is most important to control. The second aliasing regime is present when both quadratic and cubic terms alias, i.e. where $2k_p > N/2$ or $3k_p > 3N/4$ so that $2k_p = N/2 + \xi$ and

$$\begin{aligned}(k_p + k_p + k_p) &= \frac{3}{2}\left(\frac{N}{2} + \xi\right)\\ (k_p + k_p)^\diamond &= \left(\frac{-N}{2} + \xi\right)\\ (k_p + k_p + k_p)^\circ &= \left(\frac{-N}{4} + \frac{3}{2}\xi\right)\end{aligned} \tag{42}$$

in this case

$$k^* = \alpha\left(\frac{-N}{4} + \frac{3}{2}\xi\right) + 3\beta\left(\frac{-N}{2} + \xi\right) + (1 - \alpha - 2\beta)\left(\frac{3N}{4} + \frac{3\xi}{2}\right) = c_2 \tag{43}$$

where c_2 is k^* for $3N/4 < 3k_p \leqslant 3N/2$. From (41) and (43), the expressions for k^* in the two aliasing regions are

$$c_1 = \frac{(1 - 2\alpha)N}{2} + \xi, \qquad c_2 = \frac{(3 - 4\alpha - 12\beta)N}{4} + \frac{3}{2}\xi \tag{44}$$

With this, the convective operators given in Table 2 may be constructed. Writing this as $k^* = k^*(k)$,

$$\begin{aligned}k^* &= k, \quad 0 \geqslant k \geqslant \frac{N}{2}\\ k^* &= \frac{-N}{2} + \frac{(1 - 2\alpha)N}{2} + k, \quad \frac{N}{2} < k \geqslant \frac{3N}{4}\\ k^* &= \frac{-9N}{8} + \frac{(3 - 4\alpha - 12\beta)N}{4} + \frac{3k}{2}, \quad \frac{3N}{4} < k \geqslant \frac{3N}{2}\end{aligned} \tag{45}$$

Optimizing (45) entails solving for α and β. The equation for k^* with k in the range $N/2 < k \geqslant 3N/4$ is the same as in the quadratic case, i.e. $\alpha = 1/2$. For the region where $3N/4 < k \geqslant 3N/2$, k is chosen to be the lowest possible wavenumber $k = 3N/4$. This is where the most energy is likely to reside. Then $(3 - 4\alpha - 12\beta)N/4 = 0$ is used to solve for β. The resulting operator is achieved by setting $\alpha = 1/2$ and $\beta = 1/12$. Figs. 2–6 show k^* versus k for various values of α and β. This heuristic aliasing analysis implies that, in order to reduce to a minimum unphysical energy transfer and growth at the high wavenumbers, convective formulations with α and β set to values near $\alpha = 1/2$ and $\beta = 1/12$ should be employed. The detailed form of the NSE implementation used in this study is given in Appendix A.

In Section 3 results from numerical experiments performed with a direct numerical simulation (DNS) code are reported in an attempt to evaluate the performance, in practical test cases, of the different convective formulations. A comparison of the preceding heuristic analysis with the numerical results is performed in order to establish the optimal de-aliasing formulations that represents a compromise between computational cost and de-aliasing behavior, giving acceptable k^* levels over the whole range of aliased wavenumbers. Because the preceding analysis is of a heuristic nature, a further digression into the Fourier analysis [10] of finite-difference derivative operators [15] applied to quadratic and cubic terms is not considered.

Extending these ideas to quarticly or quinticly nonlinear operators by example of the cubically nonlinear operator, (33), is rewritten as

$$\nabla(fgh) = \alpha\nabla(fgh) + \beta[f\nabla(gh) + g\nabla(fh) + h\nabla(fg)] + \gamma[gh\nabla f + fh\nabla g + fg\nabla h] \tag{46}$$

where

$$\gamma = \left[1 - \binom{n-1}{0}\alpha - \binom{n-1}{1}\beta\right] \tag{47}$$

and $n = 3$ in the cubic case. The cubic, quadratic, and linear terms are each composed of $\binom{n}{0}$, $\binom{n}{1}$, and $\binom{n}{2}$ terms, respectively where $\binom{n}{i}$ represents a binomial coefficient. Each group of terms contains all possible permutations of the elemental variables. This new operator gives rise to a modified wavenumber

Table 2
Coefficients of (33) where $\gamma = (1 - \alpha - 2\beta)$ along with the particular values of k^* for aliased wavenumber regions c_1 and c_2

Case	α	β	γ	c_1	c_2
3	α	β	γ	$\frac{(1-2\alpha)N}{2} + \xi$	$\frac{(3-4\alpha-12\beta)N}{4} + \frac{3}{2}\xi$
3a	0	0	1	$\frac{N}{2} + \xi$	$\frac{3N}{4} + \frac{3}{2}\xi$
3b	0	$\frac{1}{12}$	$\frac{5}{6}$	$\frac{N}{2} + \xi$	$\frac{N}{2} + \frac{3}{2}\xi$
3c	0	$\frac{1}{6}$	$\frac{2}{3}$	$\frac{N}{2} + \xi$	$\frac{N}{4} + \frac{3}{2}\xi$
3d	0	$\frac{1}{4}$	$\frac{1}{2}$	$\frac{N}{2} + \xi$	$\frac{3}{2}\xi$
3e	0	$\frac{1}{2}$	0	$\frac{N}{2} + \xi$	$\frac{-3N}{4} + \frac{3}{2}\xi$
3f	$\frac{1}{4}$	0	$\frac{3}{4}$	$\frac{N}{4} + \xi$	$\frac{N}{2} + \frac{3}{2}\xi$
3g	$\frac{1}{4}$	$\frac{1}{12}$	$\frac{7}{12}$	$\frac{N}{4} + \xi$	$\frac{N}{4} + \frac{3}{2}\xi$
3h	$\frac{1}{4}$	$\frac{1}{6}$	$\frac{5}{12}$	$\frac{N}{4} + \xi$	$\frac{3}{2}\xi$
3i	$\frac{1}{4}$	$\frac{1}{4}$	$\frac{1}{4}$	$\frac{N}{4} + \xi$	$\frac{-N}{4} + \frac{3}{2}\xi$
3j	$\frac{1}{4}$	$\frac{1}{2}$	$\frac{-1}{4}$	$\frac{N}{4} + \xi$	$-N + \frac{3}{2}\xi$
3k	$\frac{1}{2}$	0	$\frac{1}{2}$	ξ	$\frac{N}{4} + \frac{3}{2}\xi$
3l	$\frac{1}{2}$	$\frac{1}{12}$	$\frac{1}{3}$	ξ	$\frac{3}{2}\xi$
3m	$\frac{1}{2}$	$\frac{1}{6}$	$\frac{1}{6}$	ξ	$\frac{-N}{4} + \frac{3}{2}\xi$
3n	$\frac{1}{2}$	$\frac{1}{4}$	0	ξ	$\frac{-N}{2} + \frac{3}{2}\xi$
3o	$\frac{1}{2}$	$\frac{1}{2}$	$\frac{-1}{2}$	ξ	$\frac{-5N}{4} + \frac{3}{2}\xi$
3p	$\frac{3}{4}$	0	$\frac{1}{4}$	$\frac{-N}{4} + \xi$	$\frac{3}{2}\xi$
3q	$\frac{3}{4}$	$\frac{1}{12}$	$\frac{1}{12}$	$\frac{-N}{4} + \xi$	$\frac{-N}{4} + \frac{3}{2}\xi$
3r	$\frac{3}{4}$	$\frac{1}{6}$	$\frac{-1}{12}$	$\frac{-N}{4} + \xi$	$\frac{-N}{2} + \frac{3}{2}\xi$
3s	$\frac{3}{4}$	$\frac{1}{4}$	$\frac{-1}{4}$	$\frac{-N}{4} + \xi$	$\frac{-3N}{4} + \frac{3}{2}\xi$
3t	$\frac{3}{4}$	$\frac{1}{2}$	$\frac{-3}{4}$	$\frac{-N}{4} + \xi$	$\frac{-3N}{2} + \frac{3}{2}\xi$
3u	1	0	0	$\frac{-N}{2} + \xi$	$\frac{-N}{4} + \frac{3}{2}\xi$
3v	1	$\frac{1}{12}$	$\frac{-1}{6}$	$\frac{-N}{2} + \xi$	$\frac{-N}{2} + \frac{3}{2}\xi$
3x	1	$\frac{1}{6}$	$\frac{-1}{3}$	$\frac{-N}{2} + \xi$	$\frac{-3N}{4} + \frac{3}{2}\xi$
3y	1	$\frac{1}{4}$	$\frac{-1}{2}$	$\frac{-N}{2} + \xi$	$-N + \frac{3}{2}\xi$
3w	1	$\frac{1}{2}$	-1	$\frac{-N}{2} + \xi$	$\frac{-7N}{4} + \frac{3}{2}\xi$

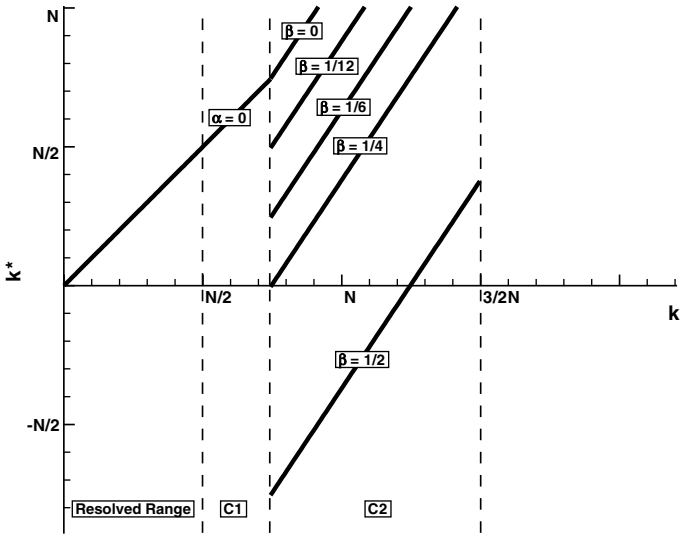

Fig. 2. Modified wavenumber k^* versus k for $\alpha = 0$ and different values of β in cubic skew-symmetric formulations.

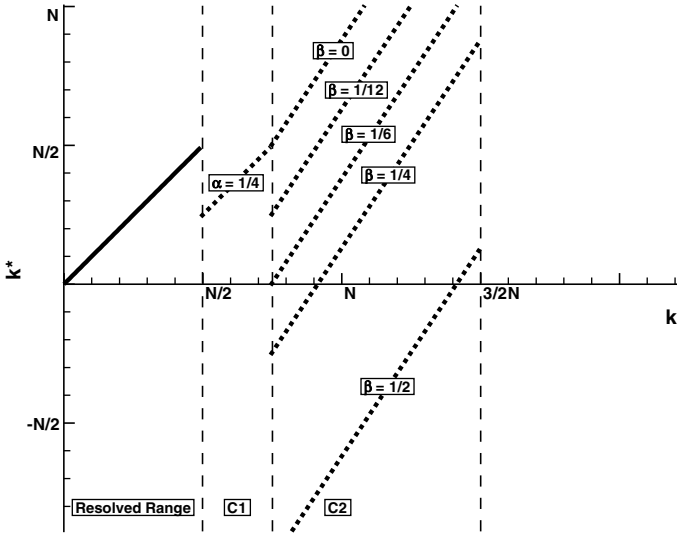

Fig. 3. Modified wavenumber k^* versus k for $\alpha = 1/4$ and different values of β in cubic skew-symmetric formulations.

$$k^* = \binom{n}{0}\alpha(n-0)k_p^{\circ} + \binom{n}{1}\beta(n-1)k_p^{\diamondsuit} + \binom{n}{2}\gamma(n-2)k_p \tag{48}$$

for $n = 3$. One solves for the c_i, $i = 1,2$ associated with the $n-1=2$ aliasing regimes whose boundaries are defined by (1) $nk_p = N/2 + \xi$ and (2) $(n-1)k_p = N/2 + \xi$. Similarly, for quarticly nonlinear operators,

$$\begin{aligned}\nabla(efgh) = {} & \alpha\nabla(efgh) + \beta[e\nabla(fgh) + f\nabla(egh) + g\nabla(efh) + h\nabla(efg)] + \gamma[ef\nabla(gh) + gh\nabla(ef) \\ & + eg\nabla(fh) + fh\nabla(eg) + eh\nabla(fg) + fg\nabla(eh)] + \delta[fgh\nabla e + egh\nabla f + efh\nabla g + efg\nabla h]\end{aligned} \tag{49}$$

where, with $n = 4$,

$$\delta = \left[1 - \binom{n-1}{0}\alpha - \binom{n-1}{1}\beta - \binom{n-1}{2}\gamma\right] = 1 - \alpha - 3\beta - 3\gamma \tag{50}$$

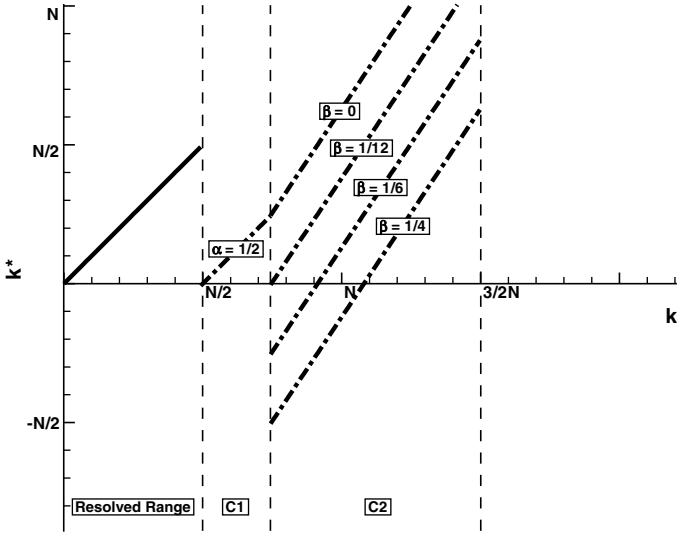

Fig. 4. Modified wavenumber k^* versus k for $\alpha = 1/2$ and different values of β in cubic skew-symmetric formulations.

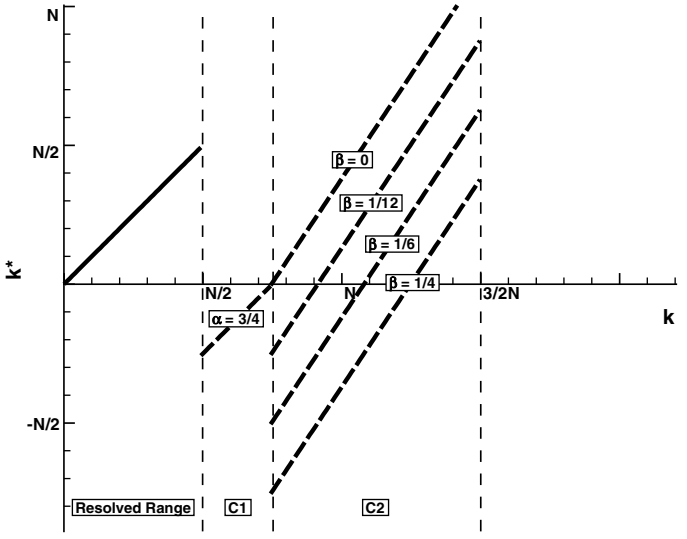

Fig. 5. Modified wavenumber k^* versus k for $\alpha = 3/4$ and different values of β in cubic skew-symmetric formulations.

and

$$k^* = \binom{n}{0}\alpha(n-0)k_p^{\square} + \binom{n}{1}\beta(n-1)k_p^{\circ} + \binom{n}{2}\gamma(n-2)k_p^{\diamondsuit} + \binom{n}{3}\delta(n-3)k_p \tag{51}$$

Therefore, one solves for the c_i, $i = 1,2,3$ associated with the $n-1=3$ aliasing regimes whose boundaries are defined by (1) $n\ k_p = N/2 + \xi$, (2) $(n-1)k_p = N/2 + \xi$, and (3) $(n-2)\ k_p = N/2 + \xi$. Just as with the cubic operator, the first regime is the most crucial; $n\ k_p = N/2 + \xi$. This procedure can be readily extended to quintically nonlinear terms and beyond.

2.3. Cost

While it is important to understand the degree to which any convective formulation results in aliased energy growth at the high wavenumbers, it is also important to consider the cost one incurs when using the different

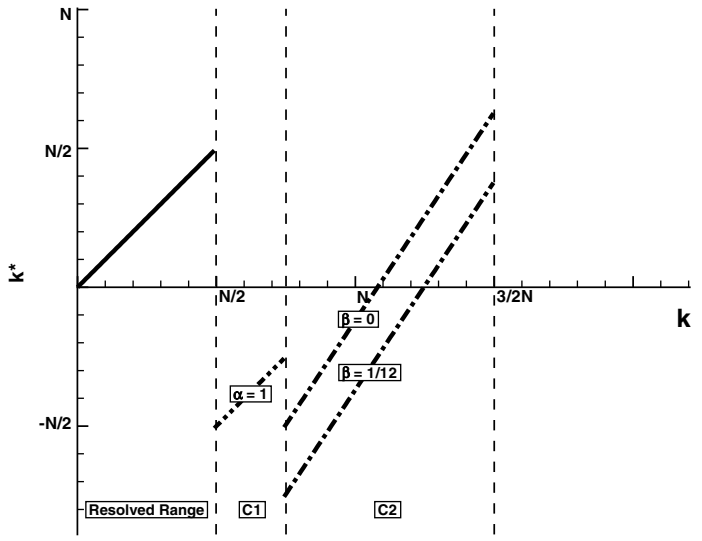

Fig. 6. Modified wavenumber k^* versus k for $\alpha = 1$ and different values of β in cubic skew-symmetric formulations.

formulations. In the previous sections, the presumed advantages of several alternative formulations of the convective terms in the Navier–Stokes equations are briefly discussed. The main problem related to the use of these formulations, especially in the context of computationally expensive high-order finite-differences operators, is the additional computations that they involve, mostly by increasing the number of costly spatial derivatives that have to be evaluated at each time step. For chemically reacting mixtures described by a large number of species N_g, an associated large number $(N_g - 1)$ of independent species conservation equations must be solved. Assuming three spatial dimensions, each one of these species conservation equations contains three convective terms, the energy and mass conservation equations contain three convective terms each, and so do each of the three momentum equations. The total number of high-order derivative operations (N_d) involved in the computation of the convective terms of the NSE in their conservative form is therefore

$$N_d = 3 \cdot 3 + 3 + 3 + 3 \cdot (N_g - 1) = 15 + 3 \cdot (N_g - 1) \tag{52}$$

where N_g is the total number of chemical species and the last term on the right-hand side of the above equation represents the cost (expressed in terms of the number of derivative operations needed) associated with the species transport equations. Likewise, the first term on the right-hand side represents the cost associated with the momentum equations, the second with continuity, the third with energy. One correction to this analysis should be made to account for how the convective operator choice is influenced by the computation of the diffusive terms. Cubic formulations and $\mathrm{QSS_F}$ require the mass fraction gradients whereas $\mathrm{QSS_B}$ does not. Since these terms are also required for the species diffusive flux, a fair comparison of the relative cost for these convective operators should consider use of mass fraction gradients as free. This is the case for the cubic operators when $\gamma \neq 0$ and $\mathrm{QSS_F}$ for the species continuity equations. With this in mind, the total cost of the quadratic and cubic convective formulations in terms of derivative operators is listed in Table 3. It is readily seen from ((9) and (10)), ((11) and (12)) and, ((53) and (54)) below, that the cost differential between these operators and a conservation/divergence approach lies principally with the species equations. The species equations generate a cost which is approximately a simple multiple of $(N_g - 1)$. These conclusions are, to some degree, solution algorithm specific.

For the test simulations of the reactive cases reported in Section 3.2, the number of species is $N_g = 9$. The cost in terms of derivative operations, N_d, almost doubles; going from $N_d = 39$ in the conservative formulation to $N_d = 78$ in the quadratic skew-symmetric $\mathrm{QSS_B}$. While for the cubic skew-symmetric formulation with $\beta = 0$ (only the linear and the purely cubic terms are retained), the cost is reduced to $N_d = 54$.

As an example of a reduced aliasing formulation, based on Table 2 and Fig. 4, we set $f = \rho$, $g = \mathbf{u}_i$ or $g = \phi$, and $h = \mathbf{u}_j$. Choosing $\alpha = 1/2$ and $\beta = 1/12$ in (33), the new operators for the momentum and scalar equations are

Table 3
Approximate number of derivative operations needed at each grid point and time step for different convective formulations to solve the RHS of (1)–(4) when $\mathbf{q}$, $\mathbf{J}_s$, τ, and $\dot{\omega}_s$ are provided

Convection operator	N_d – # of derivatives
Conservation form – (5) and (6)	$15 + 3 \cdot (N_g - 1)$
Quadratic skew-symm. F – (9), (10), and (13), $\alpha \neq 0$	$27 + 3 \cdot (N_g - 1)$
Quadratic skew-symm. B – (11)–(13), $\alpha \neq 0$	$30 + 6 \cdot (N_g - 1)$
Cubic skew-symm. – (33) $\alpha \neq 0$, $\beta = 0$	$30 + 3 \cdot (N_g - 1)$
Cubic skew-symm. – (33) $\alpha \neq 0$, $\beta \neq 0$	$51 + 9 \cdot (N_g - 1)$

$$\nabla_j \cdot (\rho \mathbf{u}_i \mathbf{u}_j) = \frac{1}{2}\nabla_j \cdot (\rho \mathbf{u}_i \mathbf{u}_j) + \frac{1}{12}[\rho \nabla_j \cdot (\mathbf{u}_i \mathbf{u}_j) + \mathbf{u}_i \nabla_j \cdot (\rho \mathbf{u}_j) + \mathbf{u}_j \cdot \nabla_j (\rho \mathbf{u}_i)] + \frac{1}{3}[\mathbf{u}_i \mathbf{u}_j \cdot \nabla_j \rho + \rho \mathbf{u}_j \cdot \nabla_j \mathbf{u}_i + \rho \mathbf{u}_i \nabla_j \cdot \mathbf{u}_j] \tag{53}$$

$$\nabla_j \cdot (\rho \phi \mathbf{u}_j) = \frac{1}{2}\nabla_j \cdot (\rho \phi \mathbf{u}_j) + \frac{1}{12}[\rho \nabla_j \cdot (\phi \mathbf{u}_j) + \phi \nabla_j \cdot (\rho \mathbf{u}_j) + \mathbf{u}_j \cdot \nabla_j (\rho \phi)] + \frac{1}{3}[\phi \mathbf{u}_j \cdot \nabla_j \rho + \rho \mathbf{u}_j \cdot \nabla_j \phi + \rho \phi \nabla_j \cdot \mathbf{u}_j] \tag{54}$$

Again, the quadratic terms on the right-hand side of both above equations add a considerable computational cost to simulations compared to the conservative formulations. A large fraction of this additional cost can be eliminated, without large increases in error, by setting $\beta = 0$ and retaining only the linear and the purely cubic terms. Hence, one has

$$\nabla_j \cdot (\rho \mathbf{u}_i \mathbf{u}_j) = \frac{1}{2}\nabla_j \cdot (\rho \mathbf{u}_i \mathbf{u}_j) + \frac{1}{2}[\mathbf{u}_i \mathbf{u}_j \cdot \nabla_j \rho + \rho \mathbf{u}_j \cdot \nabla_j \mathbf{u}_i + \rho \mathbf{u}_i \nabla_j \cdot \mathbf{u}_j] \tag{55}$$

$$\nabla_j \cdot (\rho \phi \mathbf{u}_j) = \frac{1}{2}\nabla_j \cdot (\rho \phi \mathbf{u}_j) + \frac{1}{2}[\phi \mathbf{u}_j \cdot \nabla_j \rho + \rho \mathbf{u}_j \cdot \nabla_j \phi + \rho \phi \nabla_j \cdot \mathbf{u}_j] \tag{56}$$

2.4. DNS code

A parallel Navier–Stokes solver, S3D, developed at the Combustion Research Facility (Livermore, CA), is used to perform the direct numerical simulations reported in this paper. The solution algorithm is implemented in Fortran 90. S3D solves the NSE on a structured, Cartesian mesh in three spatial directions. Chemical reactions coefficients are obtained from the CHEMKIN package [14]. Spatial derivatives are computed with an eighth-order explicit finite-difference scheme. A fourth-order, six-stage explicit Runge–Kutta scheme [16], is used for time integration paired with a proportional–integral–derivative (PID) error controller [17] to optimally adjust the time-stepping. High-order explicit spatial filters [15,23] are available in S3D from order 2 to order 20. In this paper, when filters are applied, they are order 10 filters and are only applied to the integration vector immediately after the step is completed. Filters orders above 10 could also be used effectively in the current context. Appendix A lists the implementation details of the cubic skew-symmetric operator in S3D.

3. Results

The de-aliasing performance of several different convective-term formulations in the NSE for a compressible fluid is tested by direct simulations of inert and reactive turbulent flows. The Mach number, $M = |u|/c$, represents the ratio of a characteristic convective velocity of the flow $|u|$ to the speed of sound c. A turbulent Mach number, $M_t = u'/c$, may also be defined when the characteristic convective velocity is replaced by the rms velocity fluctuation $u' = <\sqrt{\mathbf{u}' \cdot \mathbf{u}'}>$. From Passot and Pouquet [25], for very low M_t, the density fluctuations $\delta\rho/\rho$ in the flow remain negligible, the energy spectrum of the density fluctuations is flat, and the flow can be seen as essentially incompressible. As M_t increases ($0.01 < M_t < 0.3$), the density

fluctuations $\delta\rho/\rho$ increase too, the flow becomes quasi-incompressible, and the density acquires a meaningful spectrum: the flow is in the "weak Mach-number regime". For $M_t \geqslant 0.3$ shocklets make their appearances and the flow enters the "strong Mach-number regime" in which compressible effects become important and cannot be considered any longer as perturbations of a vortical flow. To assess the relative performance of the many convective formulations, numerical tests of isotropic turbulent flow in the "weak Mach-number regime" are conducted by

- varying the resolution through the chosen grid density and the integral length scale assigned to the initial turbulent flow field,
- changing the energetics of the density spectrum through the M_t assigned to the initial turbulent flow field and the presence or lack of chemical reactions,
- manipulating the convective formulation by changing the coefficients α and β.

The most obvious quality metric for a convective operator is that code does not crash. A summary of the test cases run in the context of the present work using different combinations of α and β is shown in Fig. 7. In this figure, it may be seen that a diagonal band of $\alpha - \beta$ pairs result in the DNS code not crashing. From within this banded region, still better $\alpha - \beta$ pairs exist. Other metrics chosen to evaluate the quality of a given convective formulation are the spectral behavior of relevant scalar and vector quantities like density and velocity. Also, spatially averaged values of the vorticity vector magnitude, $|\boldsymbol{\omega}| = |\nabla \times \mathbf{u}| = (\boldsymbol{\omega} \cdot \boldsymbol{\omega})^{1/2}$ and the flexion vector magnitude,$|\boldsymbol{\chi}| = |\nabla \times \boldsymbol{\omega}| = (\boldsymbol{\chi} \cdot \boldsymbol{\chi})^{1/2}$ are examined. These two terms are directly related to the more common enstrophy, $\frac{1}{2}\boldsymbol{\omega} \cdot \boldsymbol{\omega}$, and palinstrophy, $\frac{1}{2}\boldsymbol{\chi} \cdot \boldsymbol{\chi}$, terms. The flexion field [26], by virtue of its doubly differentiated form, $\boldsymbol{\chi} = \nabla \times \nabla \times \mathbf{u}$, has a wavenumber content that is far more skewed to high wavenumbers than the velocity field. Hence, the flexion magnitude is an approximate indicator of the high wavenumber content of the velocity field. It will be used to assess, in a relative sense, how much unphysical energy has accumulated at high wavenumbers over the course of the DNS runs. Instantaneous snapshots of density, temperature, and velocity fields are also used as auxiliary qualitative criteria but are not included in this paper.

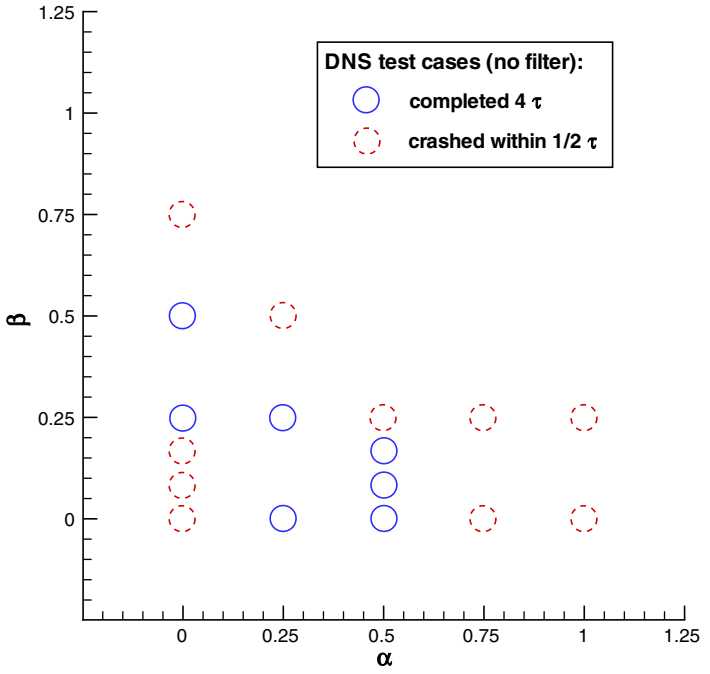

Fig. 7. Chart of the test cases for different values of the α and β coefficients.

3.1. 3-D compressible isotropic turbulence

Direct simulations of decaying isotropic compressible turbulence for an inert fluid are run at a turbulent Mach number $M_t \sim 0.2$ and at several grid resolutions. The turbulent velocity field is initialized using the Passot–Pouquet analytic expression [25]. This velocity field is computed and then mapped onto the particular grid. Simulations are run for a relatively short time interval which is the same order of magnitude of a characteristic eddy turnover time $\tau = l_t/u'$, where $l_t \sim 10^{-4}(m)$ is the integral length scale and $u' \sim 70$ (m/s) the rms velocity fluctuation. In all non-reacting flow simulations the turbulent Reynolds number is $Re_\tau = u' \cdot \rho_{\text{ref}} \cdot l_t/\mu_{\text{ref}} \sim 447$ where μ_{ref} and ρ_{ref} are the reference viscosity and density. The Kolmogorov length scale is estimated as $\eta_k \sim Re_\tau^{-3/4} \cdot l_t$ and its value is close to $10^{-4}(m)$ in the initial turbulent field. At the resolutions used in this study, simulations for turbulent Mach numbers higher than 0.3 have been attempted without success because the numerical solver is not able to properly handle shocklets that quickly form at $M_t \gtrsim 0.3$. The pressure, density, and temperature scalar fields are initialized at uniform values throughout the computational domain. However, as soon as the computations are started, the fluctuating velocity field induces fluctuations in the density, temperature, and pressure fields through the coupling intrinsic to the NSE. The number of wavenumbers available in the computational box is intentionally limited to values that do not allow a correct representation of the smallest scales of the initially imposed turbulent field. In the following text, the different resolutions used in the test cases are described using a resolution parameter, $\Gamma = \eta_k^0/\Delta_g$, where η_k^0 is the Kolmogorov length scale at time $t = 0$ and Δ_g is the grid length scale. Smaller values of Γ correspond to less resolved simulations. The value of Γ is only used to describe the initial condition.

Several test runs at resolutions $\Gamma = 0.2, 0.3, 0.9$ are performed in order to investigate the response of the unfiltered solution to different grid densities. The 3-D energy spectra of the velocity field obtained at different resolutions is shown in Fig. 8. As expected, the higher the resolution, the lower the amount of energy that is transferred to the high wavenumbers by the aliasing process. However, the previous analysis also shows that the behavior of the different convective formulations is qualitatively similar at $\Gamma = 0.2, 0.3, 0.9$. Further, smaller values of Γ are more computationally expedient in revealing the behavior of each convective operator. Accordingly, the computational domain is defined by a 32^3 grid and only the results for $\Gamma = 0.2$ are discussed.

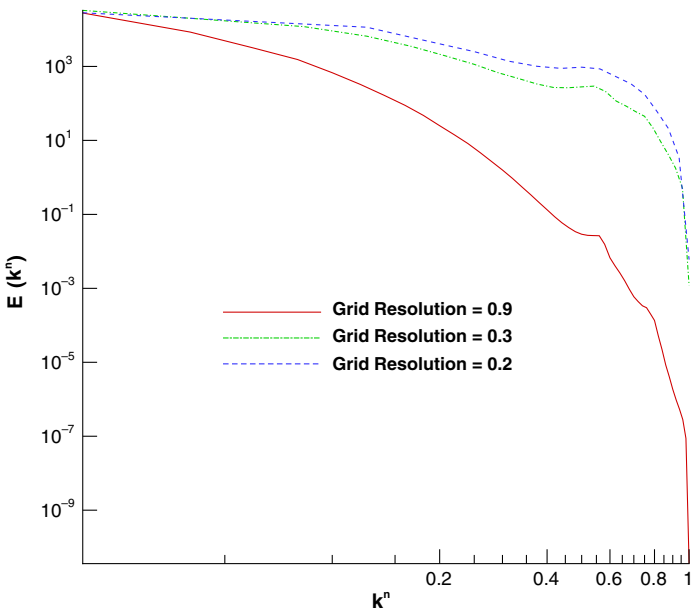

Fig. 8. Comparison of the 3-D energy spectra of the velocity field for the quadratic skew-symmetric convective formulation QSS_B at different grid resolutions ($\Gamma = 0.2, 0.3, 0.9$). The mode number $k^n = k/k_{\max}$ is normalized by the maximum number of modes supported by each grid.

At this relatively poor resolution, $\Gamma = 0.2$, a large amount of energy is initially transferred from the lower to the higher wavenumbers. Numerical tests show that the rate of this energy transfer is strongly influenced by which convective formulation is used. Typically, if the simulation survives a violent initial transient lasting for a time period of about one eddy turnover τ, a slow decay of the entire energy spectrum follows. This is the case for many of the skew-symmetric convective formulations (see Fig. 7 for an overview). In all figures below, the time is given in units of the characteristic eddy turnover time, τ.

As an example of the spectral behavior described above, the time evolution of the energy spectrum for the three-dimensional velocity field over a time period $\Delta t = 4\tau$ is shown in Fig. 9 (thick lines and circles). The time evolution of the energy spectrum for the three-dimensional scalar density field over the same time period is also shown (thin lines and diamonds). A maximum time length of $\Delta t = 4\tau$ is chosen for the simulations because such time interval is long enough for aliasing to be significant but short enough for the solution to preserve some degree of correlation with the initial turbulence field. The spectra shown in Fig. 9 results from a simulation performed using the quadratic skew-symmetric convective formulation $\mathrm{QSS_B}$, (11) and (12), and with no explicit filtering of the solution. The time evolution of the energy spectra for all other convective formulations shows the same *qualitative* behavior observed in Fig. 9; an initial large transfer of energy from the low to the high wavenumbers takes place between $t \sim 0$ and $t \sim \tau$. This initial transient is then followed by a decay over the whole range of wavenumbers between $t \sim \tau$ and $t \sim 4\tau$. However, some relevant *quantitative* differences emerge in the rate of energy transfer from the low to the high wavenumbers for the different convective formulations.

In order to formulate a more quantitative assessment about the aliasing behavior of the different convective formulations, it is convenient to compare the three-dimensional energy spectra of the velocity fields. This is done in Fig. 10 for $t \sim (1/2)\tau$ and in Fig. 11 for $t \sim 4\tau$. The combinations of α and β corresponding to the dashed circles in Fig. 7 (note that these include the conservation form of the convective terms for $\alpha = 1$ and $\beta = 0$) produced a code crash at $t \sim (1/3)\tau$ and are not included in the spectral analysis because of their poor performance. Not unexpectedly, the filtered solution (labeled Conservation – filtered) in Fig. 10 shows the lowest energy aliasing at the high wavenumbers but also a considerable energy removal from the mid-range wavenumbers ($3 < k < 7$). It should be remembered that the filter shape was chosen so as to remove only wavenumbers unresolvable by the numerical method. Given the intentional overloading of the grid, in terms of high wavenumber energy content, the amount of energy removed by the filter might appear alarming yet the removed energy was not resolvable by the numerical method. While all unfiltered solutions from the quadratic

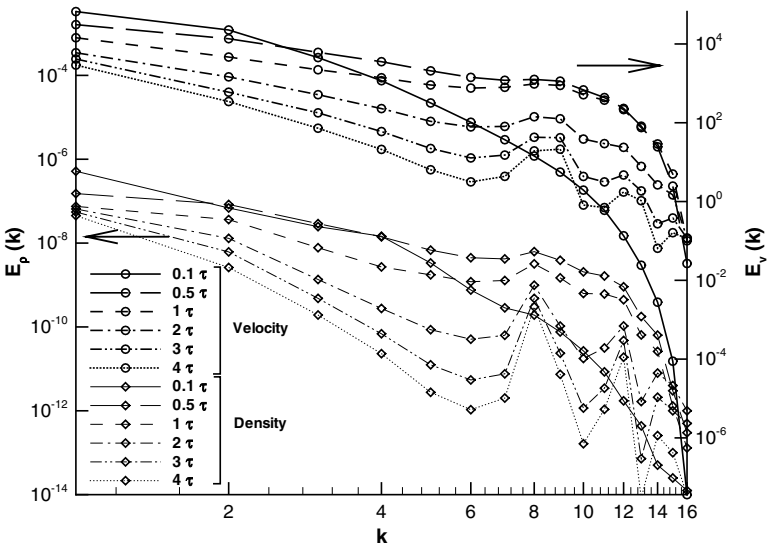

Fig. 9. Time evolution of the three-dimensional energy spectrum of the vector velocity field (thick lines and circles) and scalar density field (thin lines and diamonds) in decaying compressible isotropic turbulence. The skew-symmetric form $\mathrm{QSS_B}$ is used for the convective terms and no explicit filtering is applied to the solution.

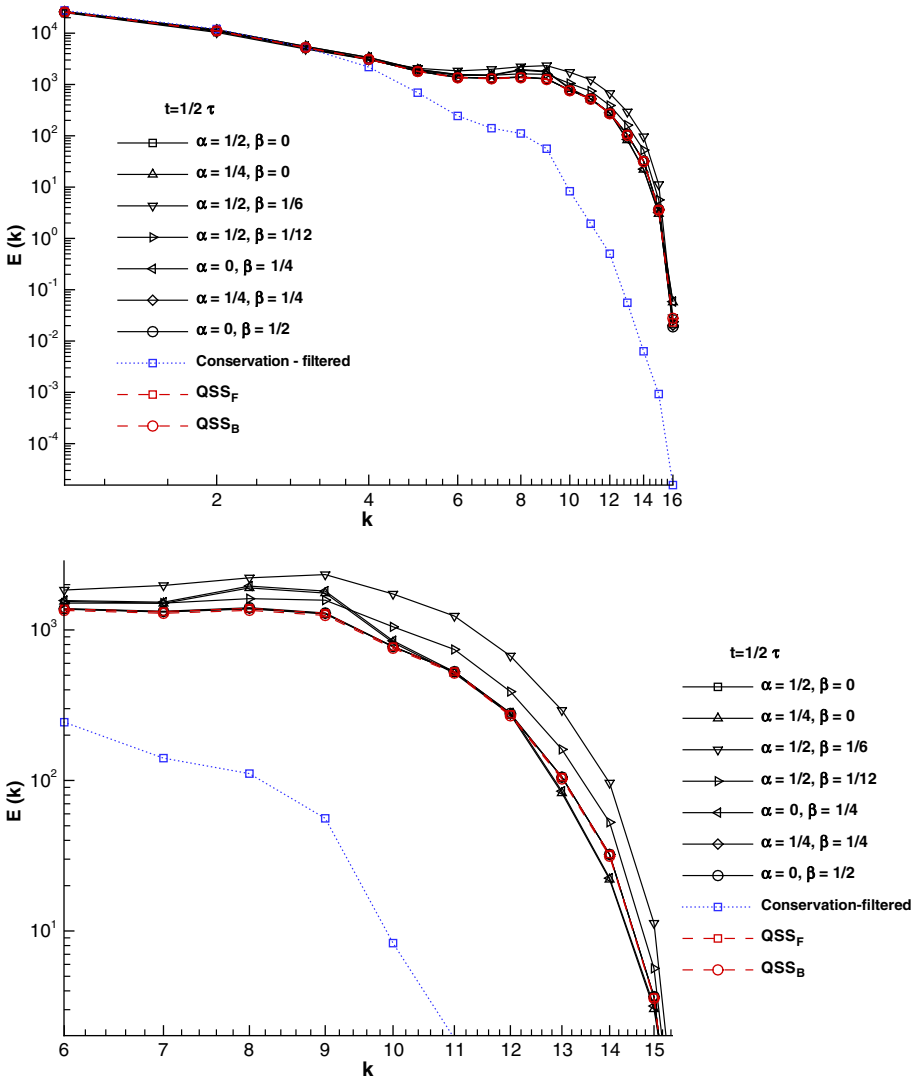

Fig. 10. Energy spectra of the 3-D velocity field for different convective formulations at $t \sim (1/2)\tau$ (top). Detail of the high wavenumbers range (bottom).

and cubic convective formulations have similar spectra, the cubic formulations having the coefficients $\alpha = 1/2$, $\beta = 1/12$ and $\alpha = 1/2$, $\beta = 1/6$ in (Section 2.2.2) are clearly characterized by the worst aliasing at $t \sim (1/2)\tau$. A detail of the top figure is shown in the bottom figure, focusing only on the range $6 < k < 16$. Note that the quadratic formulation QSS_B is characterized by a spectrum virtually indistinguishable to that of the cubic formulation obtained by setting $\alpha = 1/2$ and $\beta = 0$ in (33).

Fig. 11 shows the three-dimensional energy spectra of the velocity fields at $t \sim 4\tau$. The quadratic formulations, QSS_B and QSS_F, and the cubic formulation obtained by setting $\alpha = 1/2$ and $\beta = 0$ in (33) still show the best performance with respect to aliasing over the whole high wavenumber range $6 < k < 16$. As for the other cubic formulations, two perform relatively worse in the $6 < k < 10$ range ($\alpha = 1/4$, $\beta = 0$ and $\alpha = 0$, $\beta = 1/4$) while the other two are worse in the $10 < k < 16$ range ($\alpha = 1/2$,$\beta = 1/12$ and $\alpha = 1/2$,$\beta = 1/6$).

According to Table 2, Fig. 4, and the discussion presented in Section 2.2.2, the best de-aliasing performance of the generalized cubic convective formulation, (33), should be achieved approximately for $\alpha = 1/2$ and $\beta = 1/12$. The numerical tests confirm that $\alpha = 1/2$ is a good choice for the c_1-range but they suggest $\beta = 0$ as a better alternative for the c_2-range. This fact is somewhat surprising but nevertheless very positive, being that the

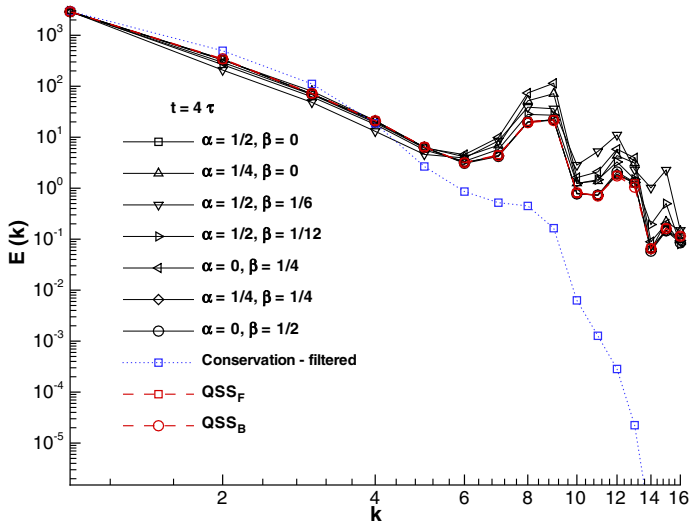

Fig. 11. Energy spectra of the 3-D velocity field for different convective formulations at $t \sim 4\tau$ in the non-reacting case.

computational cost of the numerical simulation drastically increased when $\beta \neq 0$. Hence, setting $\beta = 0$ makes the associated cubic skew-symmetric formulation of the convective terms not only preferable for minimizing unwanted energy aliasing but also for reducing operation count and computational cost.

After observing the different rates at which aliased energy builds up in the high wavenumber range for different convective formulations, it is important to then observe the time evolution of the energy contained at low wavenumbers. These are a major source from which physical energy is taken during the initial transient and transferred to the high wavenumbers by the aliasing process. The rate at which the energy decay takes place at the first wavenumber of the energy spectrum $E(k)$ for $k = 1$ is expected to be consistent with the results of Figs. 10 and 11. Examination of Fig. 12 reveals that some differences exist between the convective formulations in the time evolution of the energy content of the first wavenumber $E(1)$. Moreover, these differences are seen to increase with time.

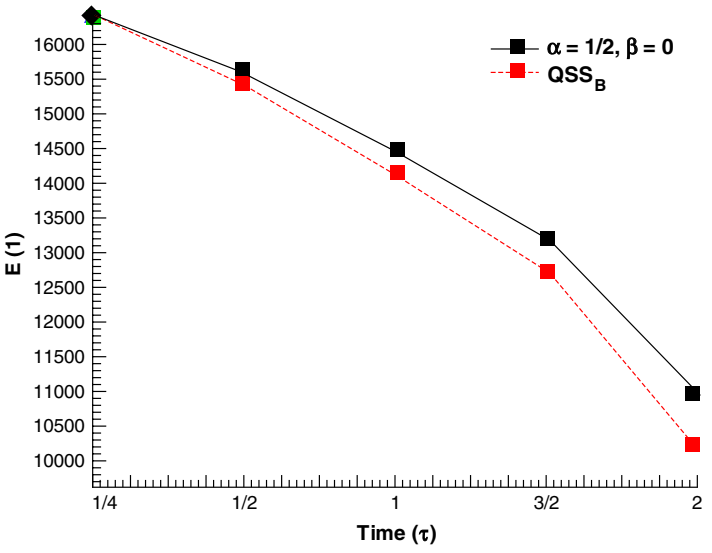

Fig. 12. Time evolution of the energy content at the first mode of the 3-D energy spectra of the velocity field for a quadratic, QSS_B, and a cubic ($\alpha = 1/2$ and $\beta = 0$) skew-symmetric convective formulation.

In comparing simulations of two convective formulations, a relatively faster decay of $E(1)$ over $0 < t < \tau$ implies a relatively faster unphysical energy transfer to higher wavenumbers through the aliasing mechanism. This may be inferred because the only difference between the two simulations is the convective formulation itself. Hence, relatively faster energy loss from low wavenumbers is indicative of poor de-aliasing behavior. Accordingly, the cubic formulation, obtained by setting $\alpha = 1/2$ and $\beta = 0$ in (33), exhibits the least aliasing in these tests.

Visual observation of the instantaneous flexion fields (not shown here) indicates that the amount of flexion in the initial turbulent field is relatively modest. However, as similar simulations proceed, the amount of flexion increases with time at a rate that depends on the particular convective formulation used. The spatially averaged values of the instantaneous vorticity magnitude, $|\boldsymbol{\omega}|$, and flexion magnitude, $|\boldsymbol{\chi}|$, at $t \sim 4\tau$ are plotted against each other in Fig. 13 for a number of different convective formulations. Lower average values of both vorticity and flexion, at $t \sim 4\tau$, are assumed to indicate lower levels of energy at the high wavenumbers of the velocity field, thus less aliasing. Accordingly, the convective formulations are assumed to perform better when closest to the bottom left of the graph. Among the inert cases (top left of Fig. 13), nearly all cubic skew-symmetric formulations show lower $|\boldsymbol{\omega}|$ and $|\boldsymbol{\chi}|$ than the quadratic one, $\mathrm{QSS_B}$, (exceptions are the combinations $\alpha = 0$, $\beta = 1/4$ and $\alpha = 1/4$, $\beta = 0$). The spectra in Fig. 11 indicate that the aliasing performance of the cubic skew-symmetric formulations corresponding to $\alpha = 0$, $\beta = 1/4$ and $\alpha = 1/4$, $\beta = 0$ are poorest in the range $6 < k < 10$ at $t \sim 4\tau$. Fig. 11 also suggests that, in a net sense, the formulations corresponding to $\alpha = 1/2$, $\beta = 1/6$ and $\alpha = 1/2$, $\beta = 1/12$, showing the lowest $|\boldsymbol{\omega}|$ and $|\boldsymbol{\chi}|$ in Fig. 13, have aliased large quantities of energy in the range $3 < k < 6$ to the highest wavenumbers range $10 < k < 16$. Therefore, one can conclude that the spatially averaged values of the vorticity and flexion magnitude, $|\boldsymbol{\omega}|$ and $|\boldsymbol{\chi}|$, are useful indicators of the level of velocity fluctuations present in the range $3 < k < 10$.

From the discussion above, the quadratic skew-symmetric convective forms, $\mathrm{QSS_B}$ and $\mathrm{QSS_F}$, and the new cubic skew-symmetric formulation obtained by setting $\alpha = 1/2$ and $\beta = 0$ in (33) result in nearly identical aliasing behavior in the case of inert decaying compressible turbulence. Interestingly, the present numerical simulations show no meaningful differences between the aliasing behavior of the quadratic skew-symmetric convective formulation of Feiereisen et al. [9], ((9) and (10)), and the alternative one proposed by Blaisdell et al. [1], corresponding to ((11) and (12)). It should be noted that this is in contrast to the conclusions reached by Erlebacher and Hussaini [7] which report a stable solution when using ((9) and (10)) and an unstable solution when ((11) and (12)) are used (both formulations use $\alpha = 1/2$).

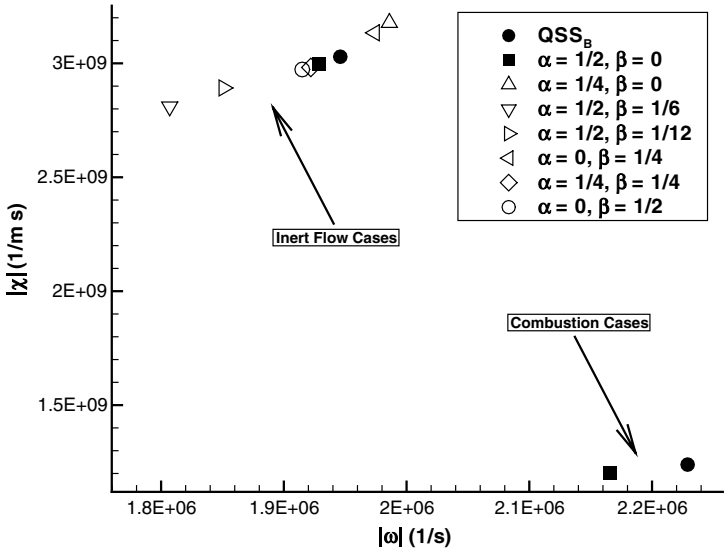

Fig. 13. Spatially averaged values of the instantaneous vorticity and flexion fields at $t \sim 4\tau$ for different convective formulations. Inert cases (upper left) and reactive cases (lower right).

3.2. 3-D premixed flame propagation in compressible decaying isotropic turbulence

The results discussed in Section 3.1 indicate that the quadratic skew-symmetric forms, QSS_B and QSS_F, and the cubic skew-symmetric form obtained by setting $\alpha = 1/2$ and $\beta = 0$ in (33) minimize aliasing error under the conditions of the tests. These three formulations result in almost identical spectral behavior, with the cubic formulation exhibiting marginally better behavior than the other two in respect to energy loss from the first wavenumber.

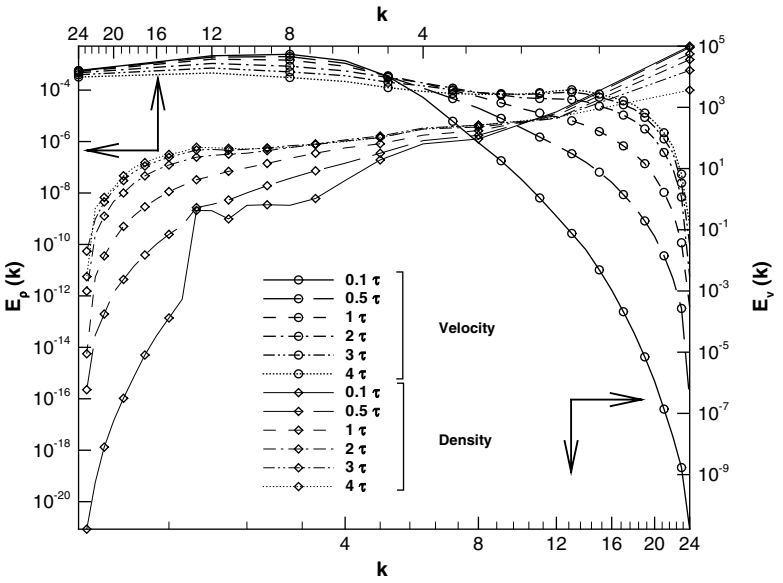

Fig. 14. Time evolution of the three-dimensional energy spectrum of the velocity vector field (thick lines and circles) and density scalar field (thin lines and diamonds) in reacting compressible turbulence. The skew-symmetric form QSS_B is used for the convective terms and no explicit filtering is applied to the solution. Note that the lower horizontal line is used for representing the velocity wavenumbers while the upper horizontal line is used for representing the density wavenumbers.

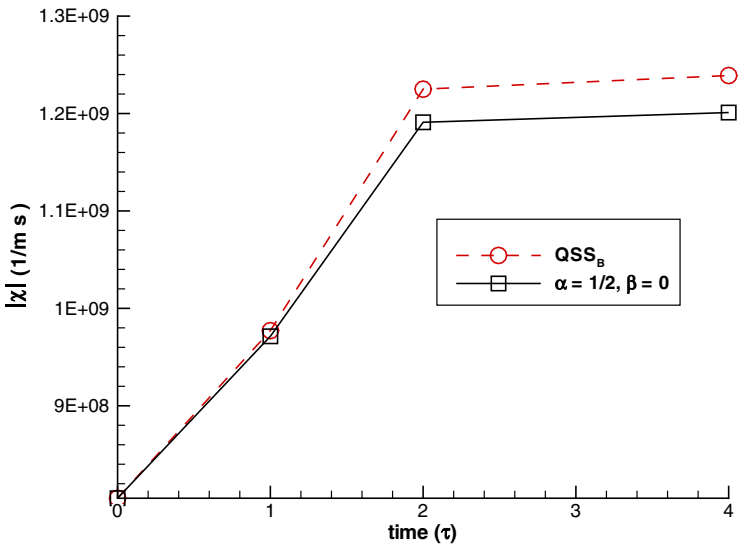

Fig. 15. Time evolution of the spatially averaged instantaneous flexion fields for the quadratic skew-symmetric convective formulation, QSS_B, and for the cubic one ($\alpha = 1/2$ and $\beta = 0$) in reacting flow.

In the present section, these three convective formulations are tested in the case of turbulent reactive flows in order to extend the conclusions reached in the previous section to the case when larger density fluctuations are present. Given the fact that the two alternative quadratic formulations result in nearly identical aliasing behavior in the reactive case also, only the QSS_B formulation, (11) and (12), is included in the following discussion.

Reactive flows are characterized by considerably stronger density variations than those observed for $M_t < 0.3$ in inert flows. One of the main ideas behind the present investigation is the hypothesis that the strong density variations found in reactive flows would enhance the cubic nature of the convective terms in the NSE, thereby making cubic skew-symmetric formulations perform relatively better with respect to aliasing.

Two parallel flat flame sheets are initially placed in the middle of the computational domain that is defined by a 48^3 grid. The flame propagates in a H_2-air mixture both in the negative and positive x-direction and creates strong temperature and density fluctuations and steep spatial gradients at the flame front. The chemical kinetics of the reacting mixture at an equivalence ratio of 1 is described by nine species and 19 reactions [20]. The ratio of

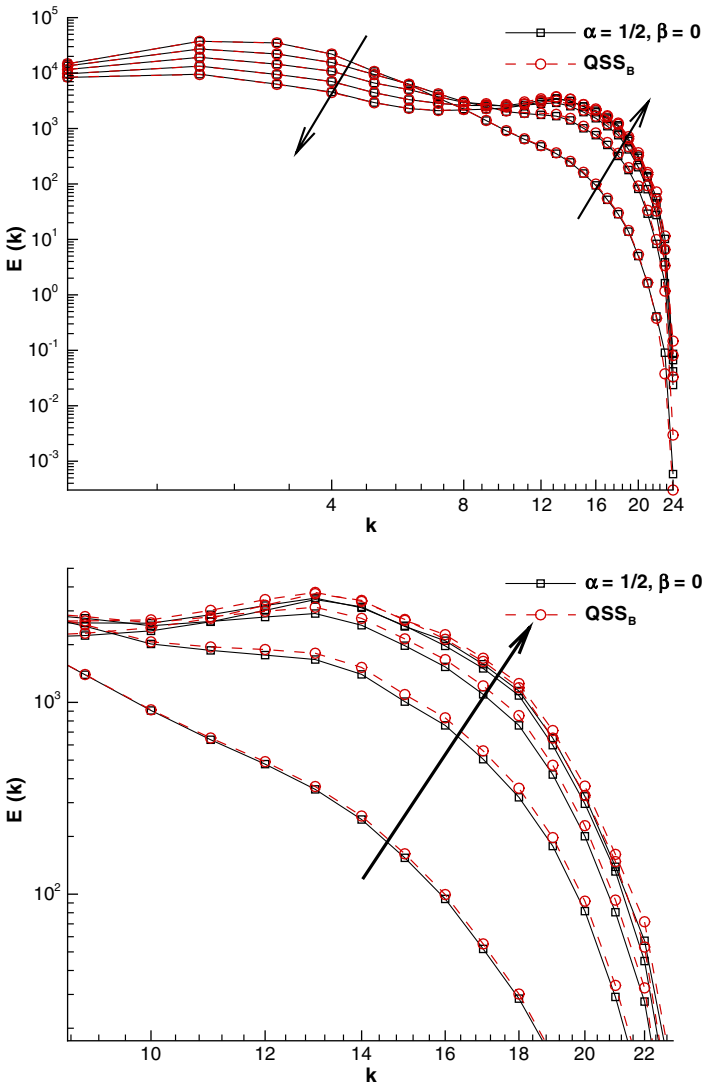

Fig. 16. Time evolution of the 3-D velocity-field energy spectra for quadratic, QSS_B, and cubic skew-symmetric convective formulations ($\alpha = 1/2$ and $\beta = 0$) from $0 \leqslant t \leqslant 4\tau$ in reacting flow. Entire wavenumber range (top) and detailed high wavenumber range (bottom). Arrows denote the direction of increasing time.

the Kolmogorov length scale to the grid length scale is set to $\Gamma = 0.2$ as in the inert cases. However, in the reactive case $Re_\tau \sim 700$ for the "cold" H_2–air mixture. Unlike the inert flow cases, the reactive flow field is aperiodic in the x-direction. This makes discrete Fourier transforms somewhat inappropriate. However, the aperiodicity was not discernable from 1-D spectra taken in the flame-normal direction (not shown here). Further details of the numerical experiment are not immediately relevant to the present discussion and are omitted.

In order to highlight the fundamental differences between the spectral behavior of the inert and reactive cases, the time evolution of the velocity spectrum, in the reactive case, over $\Delta t = 4\tau$, is shown in Fig. 14. The time evolution of the energy spectrum of the density field, over the same time period, is also shown (thin lines and diamonds). As in the inert case, a maximum time length of $\Delta t = 4\tau$ is chosen for the simulations because such time interval is long enough for aliasing to be significant but short enough for the spectra to remain reasonable and simultaneously avoiding complete combustion throughout the computational domain. Compared to the inert case, seen in Fig. 9, the density power spectrum associated to the reactive case shows a two orders of magnitude increase and no sign of decay of its energy level for wavenumbers $k > 4$ (within the simulated time interval $\Delta t \sim 4\tau$). This fact is a direct consequence of the chemical reactions that take place in the computational domain and of the associated increase in amplitude of the temperature and density fluctuations.

Visual inspection of the instantaneous velocity, vorticity, and flexion fields (not shown here) suggests that the quadratic form produces a solution characterized by smaller structures and, therefore, stronger high wavenumber fluctuations than that of the cubic form. This impression is confirmed quantitatively by the fact that, at time $t \sim 4\tau$, the mean values of vorticity and flexion averaged over the entire computational domain are larger for the quadratic case ($|\boldsymbol{\omega}| = 2.229 \times 10^6\ \mathrm{s}^{-1}$ and $|\boldsymbol{\chi}| = 1.236 \times 10^9\ \mathrm{cm}^{-1}\ \mathrm{s}^{-1}$) than for the cubic one ($|\boldsymbol{\omega}| = 2.166 \times 10^6\ \mathrm{s}^{-1}$ and $|\boldsymbol{\chi}| = 1.201 \times 10^9\ \mathrm{cm}^{-1}\ \mathrm{s}^{-1}$). This is shown at the bottom right of the graph in Fig. 13 for comparison.

For the same two convective formulations, Fig. 15 shows the time evolution of the spatially averaged value of flexion between $t \sim 0$ and $t \sim 4\tau$. After $t \sim \tau$, a lower value of $|\boldsymbol{\chi}|$ is obtained when the cubic skew-symmetric convective formulation is used. This suggests that this convective form performs better than the $\mathrm{QSS_B}$ quadratic formulation with respect to aliasing.

Fig. 16 (top) shows the time evolution of the entire energy spectrum for the three-dimensional velocity field between $t = 0$ and $t = 4\tau$ using two different convection formulations. Different amounts of aliasing to the high wavenumbers may be seen in the bottom figure which highlights the high wavenumber range from $9 < k < 23$.

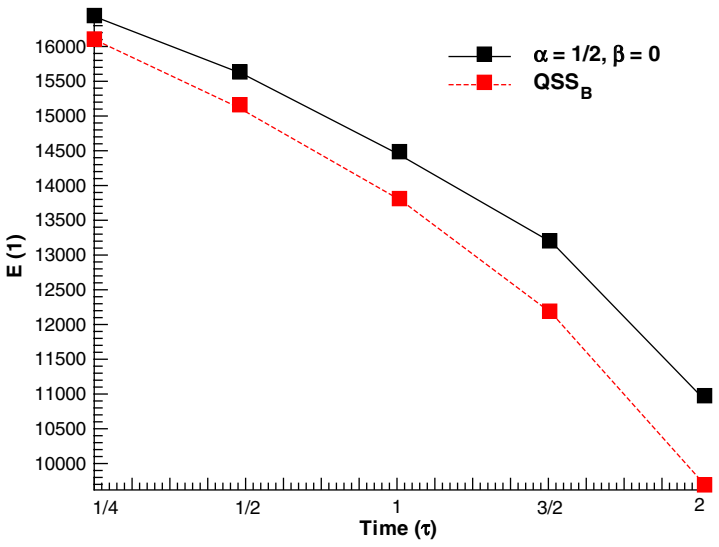

Fig. 17. Time evolution of the energy content at the first mode $E(1)$ of the 3-D energy spectra of the velocity field for a quadratic, $\mathrm{QSS_B}$, and a cubic ($\alpha = 1/2$ and $\beta = 0$) skew-symmetric convective formulation in reacting flow.

Even if the differences in the energy levels are relatively small, it is significant that they emerge in a very short time interval and generally increase as time is advanced. Again, the cubic formulation performs best.

Also in the reactive case, the rate at which the energy decay takes place at the first wavenumber of the energy spectrum, $E(1)$, is expected to be consistent with the results shown in Fig. 16 and with the discussion above. Fig. 17 reveals that the two alternative convective formulations result in significant differences in the time evolution of the energy content of $E(1)$. These differences are considerably larger than those observed in the inert cases where the density spectrum is less energetic than in the reactive case. These results suggest that while the cubic formulation with $\alpha = 1/2$ and $\beta = 0$ exhibits marginally better aliasing behavior than existing quadratic skew-symmetric formulations in flows with weak density spectra, its performance becomes appreciably better when the density spectrum broadens. Given the earlier analysis of each formulation in Section 2, this result is unsurprising.

4. Conclusions

A new family of convective operators is developed for use in the discretized form of the NSE for a compressible fluid. The essential distinction of these new convective operators, called cubic skew-symmetric convective operators, over existing approaches is that they are designed with the expectation that all three variables within the cubically nonlinear convective operator have non-trivial spectra. To investigate the efficacy of the new convective operators, the aliasing performance of several new as well as existing convective formulations is studied and compared both analytically and through numerical experiments. Analytical studies focus on the behavior of wavenumber sums with respect to what is resolvable by the grid. Unlike formulations designed with quadratic nonlinearities in mind, the aliasing performance of the new cubic operators must be analyzed in two regimes. The first, and most likely, is when the sum of the three wavenumbers aliases. Less likely, a second regime considers when the sum of two wavenumbers is sufficient to cause aliasing. From this, convective operators in (33) with values in the neighborhood of $\alpha = 1/2$ and $\beta = 1/12$ are deemed promising from a performance vantage point but the method using $\alpha = 1/2$ and $\beta = 0$ is the least computationally expensive. Numerical experiments of the new formulations investigated numerical stability, low wavenumber energy loss, and high wavenumber energy gain. As a minimal requirement of any convective operator, computational stability during the numerical experiments appeared to occur for $0.25 \lesssim (\alpha + \beta) \lesssim 0.75$. To assess the rate at which energy is aliased, the evolution of both the low and high wavenumber regimes is studied. Since much of the aliased energy is extracted from the lowest and most energetic wavenumbers, differential rates of energy loss from low wavenumbers is a useful way to compare method performance. In flows with mild density variation, the new cubic formulation with $\alpha = 1/2$ and $\beta = 0$ performed slightly better than existing quadratic skew-symmetric formulations. In reacting flows where the density spectrum is more energetic, this same cubic formulation exhibited less energy loss from low wavenumbers. Similarly, the high wavenumber energy gains were less for the new cubic formulation than existing quadratic skew-symmetric approaches. This could be seen from both velocity spectra and certain hydrodynamic variables whose values are strongly influenced by the high wavenumber energy content of the velocity field.

Better aliasing properties of the convective operator reduce the energy loss from low wavenumbers for which there is no obvious and simple remedy. Further, they reduce the accumulation of aliased energy at high wavenumbers which is generally unresolvable by the numerical method. While high-order filtering of the integration variables removes this unresolved energy content, it is preferable to mitigate the sources of aliased energy rather than to simply remove it. Also, precise filtering may be unavailable to many users. Use of the new cubic convective operator with $\alpha = 1/2$ and $\beta = 0$ results in better aliasing behavior than existing quadratic approaches, reduces the need for filtering, and does so at a lower computational cost.

Acknowledgments

The present work at SINTEF Energy Research was supported by the Norwegian Research Council. The authors are thankful to J.H. Chen of the Combustion Research Facility (Sandia National Laboratories, Livermore, CA) for granting the availability of the DNS code used to perform the numerical tests discussed in this paper.

Appendix A. Implementation

The Navier–Stokes equations for a compressible fluid are generally derived in differential form in what is called the conservation or divergence form given in (1)–(4). From these, one may rewrite various quadratic and cubically nonlinear terms using the quadratic and cubic skew-symmetric approaches, (20) and (33). Note that the continuity equation and the pressure–velocity term in the energy equation represent quadratic nonlinearities and are thus recast, unambiguously, using a quadratic skew-symmetric approach. Hence, the form of the full de-aliasing approach outlined in this paper, and as implemented in S3D, is given by

$$\begin{aligned}\frac{\partial(\rho\mathbf{u}_i)}{\partial t} &= -\nabla_j\cdot(\alpha\rho\mathbf{u}_i\mathbf{u}_j + p\delta_{ij} - \tau_{ji}) - \beta\left[\rho\nabla_j\cdot(\mathbf{u}_i\mathbf{u}_j) + \mathbf{u}_i\nabla_j\cdot(\rho\mathbf{u}_j) + \mathbf{u}_j\cdot\nabla_j(\rho\mathbf{u}_i)\right]\\ &\quad - \gamma\left[\mathbf{u}_i\mathbf{u}_j\cdot\nabla_j\rho + \rho\mathbf{u}_j\cdot\nabla_j\mathbf{u}_i + \rho\mathbf{u}_i\theta\right] + \rho\sum_{s=1}^{N_g} Y_s\mathbf{f}_{si} \qquad \text{(A.1)}\\ \frac{\partial\rho}{\partial t} &= -\nabla_j\cdot(\alpha_q\rho\mathbf{u}_j) - \beta_q\left[\rho\theta + \mathbf{u}_j\cdot\nabla_j\rho\right] \qquad \text{(A.2)}\\ \frac{\partial(\rho e_0)}{\partial t} &= -\nabla_j\cdot(\alpha\rho e_0\mathbf{u}_j + \alpha_q p\mathbf{u}_j - \tau_{ji}\cdot\mathbf{u}_i + \mathbf{q}_j) - \beta\left[\rho\nabla_j\cdot(e_0\mathbf{u}_j) + e_0\nabla_j\cdot(\rho\mathbf{u}_j) + \mathbf{u}_j\cdot\nabla_j(\rho e_0)\right]\\ &\quad - \gamma\left[e_0\mathbf{u}_j\cdot\nabla_j\rho + \rho\mathbf{u}_j\cdot\nabla_j e_0 + \rho e_0\theta\right]\\ &\quad - \beta_q\left[p\theta + \mathbf{u}_j\cdot\nabla_j p\right] + \rho\mathbf{u}_j\cdot\sum_{s=1}^{N_g} Y_s\mathbf{f}_{sj} + \sum_{s=1}^{N_g}\mathbf{f}_{sj}\cdot\mathbf{J}_{sj} \qquad \text{(A.3)}\\ \frac{\partial(\rho Y_s)}{\partial t} &= -\nabla_j\cdot(\alpha\rho Y_s\mathbf{u}_j + \mathbf{J}_{sj}) + W_s\dot{\omega}_s - \beta\left[\rho\nabla_j\cdot(Y_s\mathbf{u}_j) + Y_s\nabla_j\cdot(\rho\mathbf{u}_j) + \mathbf{u}_j\cdot\nabla_j(\rho Y_s)\right]\\ &\quad - \gamma\left[Y_s\mathbf{u}_j\cdot\nabla_j\rho + \rho\mathbf{u}_j\cdot\nabla_j Y_s + \rho Y_s\theta\right], \quad s = 1,2,\ldots,N_g \qquad \text{(A.4)}\end{aligned}$$

where $i,j = 1,2,3$, $\theta = \nabla_j\cdot\mathbf{u}_j$, $\gamma = (1-\alpha-2\beta)$, and $\beta_q = (1-\alpha_q)$. To distinguish coefficients of the cubic and quadratic skew-symmetric forms, the coefficients α, β, and γ are those of the cubic method and α_q and β_q represent those of the quadratic method. Notice that terms $\mathbf{u}_j\cdot\nabla_j\rho$ and $\nabla_j\cdot(\rho\mathbf{u}_j)$ show up several equations. Again, no attempt is made to reformulate $\nabla_j\cdot\tau_{ji}$, $\nabla_j\cdot\mathbf{q}_j$, $\nabla_j\cdot\mathbf{J}_{sj}$, and $\nabla_j\cdot(\tau_{ji}\cdot\mathbf{u}_i)$ for the purposes of enhanced aliasing performance. In S3D, while running the cubic skew-symmetric formulations, $\alpha_q = \beta_q = 1/2$ has been chosen.

References

[1] G.A. Blaisdell, N.N. Mansour, W.C. Reynolds, Numerical simulations of homogeneous compressible turbulence, Report TF-50, Thermoscience Divison, Department of Mechanical Engineering, Stanford University, Stanford, 1991.
[2] G.A. Blaisdell, E.T. Spyropoulos, J.H. Qin, The effect of the formulation of nonlinear terms on aliasing errors in spectral methods, Appl. Numer. Math. 21 (3) (1996) 207–219.
[3] J.P. Boyd, Chebychev and Fourier Spectral Methods, Dover Pub., Mineola, 2001.
[4] C. Canuto, M.Y. Hussaini, A. Quarteroni, T.A. Zang, Spectral Methods in Fluid Dynamics, Springer-Verlag, New York, 1988.
[5] F.K. Chow, P. Moin, A further study of numerical errors in large-eddy simulations, J. Comput. Phys. 184 (2) (2003) 366–380.
[6] F. Ducros, F. Laporte, T. Soulères, V. Guinot, P. Moinat, B. Caruelle, High-order fluxes for conservative skew-symmetric-like schemes in structured meshes: Application to compressible flows, J. Comput. Phys. 161 (1) (2000) 114–139.
[7] G. Erlebacher, M.Y. Hussaini, Direct numerical simulation and large eddy simulation of compressible turbulence, in: B. Galperin, S.A. Orszag (Eds.), Large Eddy Simulation of Complex Engineering and Geophysical Flows, Cambridge University Press, 1993, pp. 231–254.
[8] I. Fedioun, N. Lardjane, I. Gökalp, Revisiting numerical errors in direct and large eddy simulations of turbulence: physical and spectral spaces analysis, J. Comput. Phys. 174 (2) (2001) 816–851.
[9] W.J. Feiereisen, W.C. Reynolds, J.H. Ferziger, Numerical simulation of a compressible homogeneous, turbulent shear flow, Report TF-13, Thermoscience Division, Department of Mechanical Engineering, Stanford University, Stanford, 1981.
[10] G.B. Folland, Fourier Analysis and its Applications, Wadsworth & Brooks/Cole, Pacific Grove, 1992.
[11] B. Fornberg, On a Fourier method for the integration of hyperbolic equations, SIAM J. Numer. Anal. 12 (4) (1975) 509–528.
[12] A.E. Honein, P. Moin, Higher entropy conservation and numerical stability of compressible turbulence simulations, J. Comput. Phys. 201 (2) (2004) 531–545.

[13] K. Horiuti, T. Itami, Truncation error analysis of the rotational form for the convective terms in the Navier–Stokes equations, J. Comput. Phys. 145 (2) (1998) 671–692.
[14] R.J. Kee, G. Dixon-Lewis, J. Warnatz, M.E. Coltrin, J.A. Miller, H.K. Moffat, A Fortran Chemical Kinetics Package for the Analysis of Gas-Phase Chemical Kinetics, Reaction Design Inc., Release 3.5, San Diego, 1999.
[15] C.A. Kennedy, M.H. Carpenter, Several new numerical methods for compressible shear-layer simulations, Appl. Numer. Math. 14 (4) (1994) 397–433.
[16] C.A. Kennedy, M.H. Carpenter, R.M. Lewis, Low-storage, explicit Runge–Kutta schemes for the compressible Navier–Stokes equations, Appl. Numer. Math. 35 (3) (2000) 177–219.
[17] C.A. Kennedy, M.H. Carpenter, Additive Runge–Kutta schemes for convection–diffusion–reaction equations, Appl. Numer. Math. 44 (1–2) (2003) 139–181.
[18] A.G. Kravchenko, P. Moin, On the effect of numerical errors in large eddy simulations of turbulent flows, J. Comput. Phys. 131 (2) (1997) 310–322.
[19] S.K. Lele, Compact finite difference schemes with spectral like resolution, J. Comput. Phys. 103 (1) (1992) 16–42.
[20] J. Li, Z. Zhao, A. Kazakov, F.L. Dryer, An updated comprehensive kinetic model of hydrogen combustion, Int. J. Chem. Kin. 36 (10) (2004) 566–575.
[21] G. Lube, M.A. Olshanskii, Stable finite-element calculation of incompressible flows using the rotation form of convection, IMA J. Numer. Anal. 22 (3) (2002) 437–461.
[22] Y. Morinishi, S. Tamano, K. Nakabayashi, A DNS algorithm using B-spline collocation method for compressible turbulent channel flow, Comp. Fluids 32 (5) (2003) 751–776.
[23] J. Ray, C.A. Kennedy, S. Lefantzi, H.N. Najm, Using high-order methods on adaptively refined block-structured meshes: derivatives, interpolations, and filters, SIAM J. Sci. Comput. 29 (1) (2007) 139–181.
[24] N. Park, K. Mahesh, Analysis of numerical errors in large eddy simulation using statistical closure theory, J. Comput. Phys. 222 (1) (2007) 194–216.
[25] T. Passot, A. Pouquet, Numerical simulation of compressible homogeneous flows in the turbulent regime, J. Fluid Mech. 181 (1987) 441–466.
[26] C.A. Truesdell, Kinematics of Vorticity, Science Series, 19, Indiana University Press, Bloomington, 1954.
[27] R.W.C.P. Verstappen, A.E.P. Veldman, Symmetry-preserving discretization of turbulent flow, J. Comput. Phys. 187 (1) (2003) 343–368.
[28] D. Wilhelm, L. Kleiser, Stability analysis for different formulations of the nonlinear term in P_N–P_{N-2} spectral element discretizations of the Navier–Stokes equations, J. Comput. Phys. 174 (1) (2001) 306–326.
[29] T.A. Zang, On the rotation and skew-symmetric forms for incompressible flow simulations, Appl. Numer. Math. 7 (1) (1991) 27–40.